

The fraction and kinematics of broad absorption line quasars across cosmic time

MANUELA BISCHETTI,^{1,2} FABRIZIO FIORE,^{2,3} CHIARA FERUGLIO,^{2,3} VALENTINA D'ODORICO,^{2,3,4} NAHUM ARAV,⁵
 KASTYTIS ZUBOVAS,^{6,7} GEORGE BECKER,⁸ GUIDO CUPANI,⁹ REBECCA DAVIES,^{10,11} ANNA-CHRISTINA EILERS,¹²
 EMANUELE PAOLO FARINA,¹³ ANDREA FERRARA,¹⁴ MASSIMO GASPARI,¹⁵ CHIARA MAZZUCHELLI,¹⁶ MASAFUSA ONUYE,^{17,18}
 ENRICO PICONCELLI,¹⁹ MARIA VITTORIA ZANCHETTIN,^{20,21,2} AND YONGDA ZHU⁸

¹*Dipartimento di Fisica, Universitá di Trieste, Sezione di Astronomia, Via G.B. Tiepolo 11, I-34131 Trieste, Italy*

²*INAF - Osservatorio Astronomico di Trieste, Via G. B. Tiepolo 11, I-34143 Trieste, Italy*

³*IFPU - Institut for fundamental physics of the Universe, Via Beirut 2, 34014 Trieste, Italy*

⁴*Scuola Normale Superiore, Piazza dei Cavalieri 7, I-56126 Pisa, Italy*

⁵*Department of Physics, Virginia Tech, Blacksburg, VA 24061, USA*

⁶*Center for Physical Sciences and Technology, Saulėtekio al. 3, Vilnius LT-10257, Lithuania*

⁷*Astronomical Observatory, Vilnius University, Saulėtekio al. 3, Vilnius LT-10257, Lithuania*

⁸*Department of Physics & Astronomy, University of California, Riverside, CA 92521, USA*

⁹*INAF - Osservatorio Astronomico di Trieste, Via G. B. Tiepolo 11, I-34143 Trieste, Italy*

¹⁰*Centre for Astrophysics and Supercomputing, Swinburne University of Technology, Hawthorn, Victoria 3122, Australia*

¹¹*ARC Centre of Excellence for All Sky Astrophysics in 3 Dimensions (ASTRO 3D), Australia*

¹²*MIT Kavli Institute for Astrophysics and Space Research, 77 Massachusetts Ave., Cambridge, MA 02139, USA*

¹³*Gemini Observatory, NSF's NOIRLab, 670 N A'ohoku Place, Hilo, Hawai'i, 96720, USA*

¹⁴*Scuola Normale Superiore, Piazza dei Cavalieri 7, I-56126 Pisa, Italy*

¹⁵*Department of Astrophysical Sciences, Princeton University, Princeton, NJ 08544, USA*

¹⁶*Instituto de Estudios Astrofísicos, Facultad de Ingeniería y Ciencias, Universidad Diego Portales, Avenida Ejército Libertador 441, Santiago, Chile*

¹⁷*Kavli Institute for Astronomy and Astrophysics, Peking University, Beijing 100871, China*

¹⁸*Kavli Institute for the Physics and Mathematics of the Universe (Kavli IPMU, WPI), The University of Tokyo, Chiba 277-8583, Japan*

¹⁹*INAF - Osservatorio Astronomico di Roma, via Frascati 33, 00040, Monte Porzio Catone, Italy*

²⁰*SISSA, Via Bonomea 265, 34136, Trieste, Italy*

²¹*Dipartimento di Fisica, Sezione di Astronomia, Universitá di Trieste, via Tiepolo 11, 34143 Trieste, Italy*

ABSTRACT

Luminous quasars are powerful targets to investigate the role of feedback from supermassive black-holes (BHs) in regulating the growth phases of BHs themselves and of their host galaxies, up to the highest redshifts. Here we investigate the cosmic evolution of the occurrence and kinematics of BH-driven outflows, as traced by broad absorption line (BAL) features, due to the C IV ionic transition. We exploit a sample of 1935 quasars at $z = 2.1 - 6.6$ with bolometric luminosity $\log(L_{\text{bol}}/\text{erg s}^{-1}) \gtrsim 46.8$, drawn from the Sloan Digital Sky Survey and from the X-shooter legacy survey of Quasars at Reionisation (XQR-30). We consider rest-frame optical bright quasars to minimise observational biases due to quasar selection criteria and we apply a homogeneous BAL identification analysis, based on employing composite template spectra to estimate the quasar intrinsic emission. We find a BAL quasar fraction close to 20% at $z \sim 2 - 4$, while it increases to almost 50% at $z \sim 6$. The velocity and width of the BAL features also increase at $z \gtrsim 4.5$. We exclude that the redshift evolution of the BAL properties is due to differences in terms of quasar luminosity and accretion rate. These results suggest significant BH feedback occurring in the 1 Gyr old Universe, likely affecting the growth of BHs and, possibly, of their host galaxies, as supported by models of early BH and galaxy evolution.

Corresponding author: Manuela Bischetti
 manuela.bischetti@inaf.it

Keywords: Supermassive black holes (1663) — Quasars(1663) — Broad-absorption line quasar(183) — High-redshift galaxies(734) — Galaxy evolution(594)

1. INTRODUCTION

Quasars are the brightest, non-transient sources in the Universe. They are powered by accretion onto supermassive black holes (BHs), whose emission typically dominates over the host-galaxy emission in the rest-frame UV and optical bands. High-redshift quasars at $z \simeq 2 - 6.5$ provide a unique window on the growth phases during which the most massive BHs and their host-galaxies assembled the bulk of their mass (Marconi et al. 2004; Volonteri & Rees 2006). Luminous quasars at $z \gtrsim 2$, with bolometric luminosity $L_{\text{Bol}} \gtrsim 10^{47}$ erg/s, are typically powered by BHs with masses of $10^8 - 10^{10}$ M_{\odot} yr^{-1} and high accretion rates $\lambda_{\text{Edd}} = L_{\text{Bol}}/L_{\text{Edd}} \sim 0.01 - 1$ (e.g. Kurk et al. 2007; Shen et al. 2011; Mazzucchelli et al. 2017), where L_{Edd} is the Eddington luminosity. The large radiative output of these BHs is expected to drive powerful outflows, able to regulate the BH and host-galaxy growth, by injecting large amounts of energy and momentum in the galaxy interstellar medium (ISM, Zubovas & King 2012; Gaspari & Sadowski 2017; Menci et al. 2019).

A powerful tool to probe BH-driven outflows in quasars are broad ($> 2,000$ km s^{-1}) absorption line (BAL) systems occurring in the rest-frame UV spectrum (Weymann et al. 1991), blueward of high-ionisation emission lines such as C IV $\lambda 1,549\text{\AA}$, Si IV $\lambda 1,397\text{\AA}$, N V $\lambda 1,240\text{\AA}$ (HiBAL), and of low-ionisation emission lines such as Mg II $\lambda 2,800\text{\AA}$ (LoBAL). BAL features have been indeed identified in quasars at all redshifts up to $z > 7$ (Wang et al. 2018, 2021a). Observational studies, mostly based on spectra from the Sloan Digital Sky Survey (SDSS), found that BAL outflows are observed in 10-17% of $z \simeq 2 - 4$ quasars, and have typical velocities of 5,000-10,000 km/s (Gibson et al. 2009; Páris et al. 2018), although a few percent of them can reach 10 – 15% of the light speed (Hamann et al. 2018; Bruni et al. 2019; Rodríguez Hidalgo et al. 2020). LoBAL outflows are typically observed in a small fraction (10 – 15 %) of BAL quasars.

In luminous quasars at $z \simeq 2 - 3$, BAL outflows have been found to carry kinetic power values in the range 0.1-10% of L_{Bol} (Dunn et al. 2010; Borguet et al. 2013; Byun et al. 2022), consistent with expectations for an efficient BH-feedback mechanism (Fiore et al. 2017). Similarly, galaxy evolution models identify BAL outflows as an important source of feedback (e.g. Costa et al. 2014; Torrey et al. 2020). Different scenarios for the launching and geometry of BAL outflows have been proposed

(Elvis 2000; Proga et al. 2000; Proga & Kallman 2004; Xu et al. 2020; Zeiliger-Hess et al. 2020). Although these winds are expected to originate within a pc from the BH (Sadowski & Gaspari 2017), close to the accretion disc, observations indicate that BAL absorption in luminous quasars often occurs at much larger distances from the BH, that is 100-1,000 pc (Arav et al. 2018; Hemler et al. 2019). This suggests that these ionised outflows represent an important source of BH feedback on the growth of the BH itself and of the host-galaxy.

At very high redshift ($z \gtrsim 6$), the occurrence and properties of BAL quasar outflows are much less explored. The number of discovered BAL quasars has kept increasing with the growing number of quasars with spectroscopic observations of enough quality and enough spectral coverage to probe at least the most prominent BAL features. A first guess for a BAL quasar fraction as high as 50% at $z \sim 6$ had been previously suggested by Maiolino et al. (2004), based on a very small sample of eight quasars. A BAL fraction of 16-24 % was later reported by Shen et al. (2019); Schindler et al. (2020); Yang et al. (2021), although the BAL identification was mostly based on visual inspection and/or limited spectral range and SNR of the quasar spectra. In Bischetti et al. (2022), we have recently performed the first systematic investigation of BAL outflows in 30 quasars at $5.8 \leq z \leq 6.6$ from the X-shooter legacy survey of Quasars at the Reionisation epoch (XQR-30, Zhu et al. 2021, 2022; Bosman et al. 2021; Lai et al. 2022; Chen et al. 2022). The XQR-30 survey has indeed provided homogenous, high-sensitivity spectroscopy of a representative sample of luminous quasars at $z \sim 6$. About 40-47% of XQR-30 quasars show BAL features associated with C IV, a fraction that is ~ 2.4 times higher than what observed in $z \sim 2 - 4$ quasars (Bischetti et al. 2022). The majority of BAL outflows at $z \sim 6$ also show extreme velocities of 20,000-50,000 km s^{-1} , rarely observed at lower redshift. These results indicate that BAL outflows in $z \sim 6$ quasars inject on average large amounts of energy in their surroundings and may represent an important source of BH feedback at early epochs (Bischetti et al. 2022). These findings also indicate that high-z ($z \sim 6$) and low-z ($z \sim 2 - 4.5$) quasars may be different in terms of BAL properties.

However, different factors such as L_{Bol} or λ_{Edd} are believed to affect the fraction of BAL quasars and their kinematics (e.g. Dai et al. 2008; Allen et al. 2011; Bruni et al. 2019). In this paper we investigate the BAL frac-

tion and the BAL kinematics dependence on redshift and on quasar nuclear properties (L_{Bol} , λ_{Edd}), with the goal of identifying the main driver of the varying BAL properties. To this purpose, we measure the occurrence and kinematic properties of BAL outflows associated with the C IV ionic species in a sample of luminous quasars in the redshift range $z = 2.1 - 6.6$ (Bischetti et al. 2022), with matched selection criteria, and by adopting a homogeneous BAL identification analysis.

The paper is structured as follows. In Sect. 2, we describe the quasar sample, including quasar selection criteria (Sect. 2.1). Section 3 details the BAL identification analysis and compares it with previous approaches. The main results on the BAL fraction and on the BAL kinematics are presented in Sect. 4 and Sect. 5, respectively. We discuss the cosmic evolution of the BAL properties and its implications for BH and galaxy evolution in Sect. 6. A summary and the main conclusions are given in Sect. 7. Throughout this paper, we adopt a Λ CDM cosmology with $H_0 = 67.3 \text{ km s}^{-1}$, $\Omega_\Lambda = 0.69$ and $\Omega_M = 0.31$ (Planck Collaboration et al. 2016).

2. QUASAR SAMPLE

2.1. Quasar selection

The observed fraction of BAL with respect to non-BAL quasars is the convolution of the intrinsic BAL quasar occurrence and a quasar selection function. Standard quasar selection algorithms in optical surveys rely on multicolor imaging data which probe the rest-frame UV quasar spectrum at $z > 2$ (e.g. Richards et al. 2002). These UV colors can be affected by BAL troughs associated with high-ionisation species such as C IV. In addition, BAL quasars typically show redder UV continua than non-BAL quasars (e.g. Reichard et al. 2003; Gibson et al. 2009). Depending on redshift, BAL quasars may thus show UV colors resembling those of stars, and may be more easily missed by spectroscopic samples than non-BAL quasars.

Aiming to measure the intrinsic fraction of BAL quasars across cosmic time, two main approaches can be followed. One possibility is to translate the observed BAL fraction (f_{obs}) into an intrinsic fraction (f_{int}) by correcting for selection effects. Previous attempts to correct for these effects, however, resulted in very different f_{int} (by a factor of three), and different f_{obs} to f_{int} corrections (by a factor of five), even considering the same set of selection effects, and similar redshift intervals (Table 1). When considering SDSS quasars, Reichard et al. (2003) found $f_{\text{int}} = 13.4 \pm 1.2\%$ ($f_{\text{obs}} = 14.0 \pm 1.0\%$), Knigge et al. (2008) reported $f_{\text{int}} \leq 23\%$ ($f_{\text{obs}} = 13.7 \pm 0.3\%$), while Gibson et al. (2009) derived $f_{\text{int}} = 16.4 \pm 0.6\%$ or $18.5 \pm 0.7\%$ considering different

Table 1. BAL fraction estimates at $2 < z < 4$

Reference	f_{obs}	f_{int}
(1)	(2)	(3)
Reichard et al. (2003)	$14.0 \pm 1.0\%$	$13.4 \pm 1.2\%$
Knigge et al. (2008)	$13.7 \pm 0.3\%$	$\leq 23\%$
Gibson et al. (2009)	$15.1 \pm 0.6\%$	$18.5 \pm 0.7\%$
Allen et al. (2011)	$8.0 \pm 0.1\%$	$40.7 \pm 5.4\%$
Hewett & Foltz (2003)	$15 \pm 3\%$	$22 \pm 4\%$
Dai et al. (2008)	$\sim 20\%$	$23 \pm 3\%$
Ganguly & Brotherton (2008)	23%	—
Maddox et al. (2008)	17.5	18.5%

NOTE—(1) Reference, (2) observed BAL fraction, (3) intrinsic BAL fraction (see Sect. 2.1). The horizontal line separates UV selected (above) and optically selected (below) quasar samples.

reddening values ($f_{\text{obs}} = 15.1 \pm 0.6\%$). A higher f_{int} was reported by Allen et al. (2011): $38.8 \pm 2.2\%$ at $z < 2.3$ and $40.7 \pm 5.4\%$ at $z > 3$ ($f_{\text{obs}} = 8.0 \pm 0.1\%$). Based on the Large Bright Quasar Survey, Hewett & Foltz (2003) reported a $f_{\text{int}} = 22 \pm 4\%$ ($f_{\text{obs}} = 15 \pm 3\%$). In all these cases, the derived f_{int} mostly depends on the adopted assumptions on the input BAL properties, such as the distributions of the velocity, width and depth of the absorption, and on the relation between the above quantities and reddening. The spread of plausible assumptions naturally leads to large uncertainties. The true f_{int} could in principle be derived by quantifying the selection effects on a set of synthetic spectra based on a physical model of BAL quasar outflows. Such an approach would nonetheless suffer from large uncertainties, due to the lack of a self-consistent physical model, able to widely reproduce the properties of the BAL quasar population (e.g. Elvis 2000; Xu et al. 2020).

In this work, we follow a different approach that allows us to bypass the above issues. As we are mainly interested in the redshift evolution of the BAL fraction and kinematic properties, we apply a similar selection function at all redshifts. In particular, we consider rest-frame optically bright quasars to measure the BAL fraction in the redshift interval $z \simeq 2 - 6.5$. At $z \simeq 2 - 4$, the rest-frame optical band is probed by near-infrared surveys such as 2MASS (Skrutskie et al. 2006) and UKIDSS (Warren et al. 2007) in the H and K bands. For higher redshift quasars ($z \sim 6$), a similar spectral coverage is provided by WISE (Wright et al. 2010) in the W1 and W2 bands (see Bischetti et al. 2022, for details). The rest-frame optical selection allows us

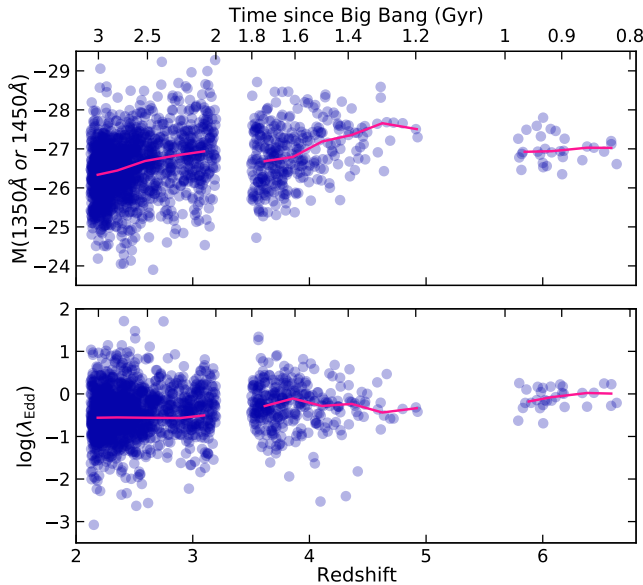


Figure 1. Absolute magnitude (top) and Eddington accretion rate (bottom) as a function of redshift for the quasar sample considered in this work. Top axis indicates time since Big Bang. Magenta line represents the median magnitude in redshift bins $\Delta z = 0.25$.

to minimise selection effects by avoiding those biases generated by UV absorption troughs in the colour selection. The f_{obs} -to- f_{int} correction in rest-frame optical selected quasars is indeed expected to be modest (10–20%): [Dai et al. \(2008\)](#) found a $f_{\text{int}} = 23 \pm 3\%$ in SDSS and 2MASS, K-band bright quasars at $z \simeq 2 - 4$ ($f_{\text{obs}} \sim 20\%$). This fraction is similar to that found by [Ganguly et al. \(2007\)](#) and [Ganguly & Brotherton \(2008\)](#) when combining SDSS and 2MASS catalogs (23%). Again, [Maddox et al. \(2008\)](#) reported a $f_{\text{int}} = 18.5\%$ in SDSS and UKIDSS bright quasars, considering the fraction of quasars missed by the UKIDSS survey ($f_{\text{obs}} = 17.5\%$). As a general trend, the observed BAL fraction calculated in rest-frame optical selected quasars is roughly 50% higher than the BAL fraction observed in quasars selected only in the rest-frame UV: $f_{\text{obs}}^{\text{optical}} \simeq 1.5 \times f_{\text{obs}}^{\text{UV}}$. In addition, the observed and intrinsic BAL fraction calculated in rest-frame optical selected quasars are similar. They are also similar to the intrinsic BAL fraction calculated in quasars selected only in the rest-frame UV: $f_{\text{obs}}^{\text{optical}} \simeq f_{\text{int}}^{\text{optical}} \sim f_{\text{int}}^{\text{UV}}$.

The f_{obs} of quasar samples selected from X-ray to radio surveys, affected by a variety of different selection effects, is typically lower or similar to 20% (e.g. [Giusettini et al. 2008](#); [Becker et al. 2000](#)), supporting the fact that most BAL quasars are recovered by a rest-frame optical selection. In general, BAL fractions higher than 20% have been reported only i) when considering the absorption index criterion (AI, [Hall et al. 2002](#), considering

troughs wider than 1,000 km/s) to identify BAL quasars, instead of the balnicity index criterion considered in this work (BI, [Weymann et al. 1991](#), see Sect. 3.2). Using $AI > 0$ typically results in a two times higher BAL fraction than using $BI > 0$ ([Dai et al. 2008](#)); ii) in the reddest quasars ([Urrutia et al. 2008](#); [Glikman et al. 2012](#)), which however constitute a minority ($\sim 10\%$) of the rest-frame optical selected quasars.

Given the above evidence, the BAL fractions presented in this work and their redshift evolution are robust against selection effects.

2.2. $2.1 < z < 5.0$ sample

The low-redshift sample consists of 1578 quasars at $2.13 < z < 3.20$ from the catalogue of SDSS DR7 quasars by [Shen et al. \(2011\)](#), selected to be detected by 2MASS in the H($1.7\mu\text{m}$) and K($2.2\mu\text{m}$) bands, which cover rest-frame optical regions of the quasar spectrum, similar to those probed by W1 and W2 in the high-redshift sample. We also include 327 SDSS DR7 quasars at $3.6 < z < 5.0$ from the [Shen et al. \(2011\)](#) catalogue, requiring them to be detected in the 2MASS K band (which correspond to W1 at $z \sim 6$). These quasars are about a factor of ten more luminous than the average SDSS quasar at $z > 2.13$, with a median magnitude of $M_{1450\text{\AA}} = -26.6$ (-26.5 at $z < 3.2$, -26.9 at $3.6 < z < 5$, Fig. 1). Their spectra have a typical SNR ~ 18 per 70 km s^{-1} pixel in the $1500 - 1600 \text{ \AA}$ range. This sample benefits from measured black hole masses ([Shen et al. 2011](#)), which are based on the Mg II line for $z \lesssim 2.3$ quasars and on the C IV emission line at $z > 2.3$, including the empirical correction for non-virial motions by [Coatman et al. \(2017\)](#). For the subsample of quasars already discovered by SDSS DR5, the occurrence and properties of BAL outflows were investigated by [Gibson et al. \(2009\)](#), providing us with a reference analysis to test our BAL identification method. For the remaining quasars, BAL identification in the catalogue was based on visual inspection ([Shen et al. 2011](#)). In this work and in [Bischetti et al. \(2022\)](#), we have re-analysed all SDSS quasars in the $2.1 < z < 5.0$ sample, following the approach described in Sect. 3.

2.3. $5.8 < z < 6.6$ sample

The high-redshift sample used in this work consists of 30 luminous quasars (median AB magnitude $M_{1450\text{\AA}} = -26.9$) at $5.8 \lesssim z \lesssim 6.6$ from the XQR-30 survey. Their magnitude and redshift distributions are shown in Fig. 1 ([Bañados et al. 2016](#); [Mazzucchelli et al. 2017](#); [Reed et al. 2017](#); [Decarli et al. 2018](#); [Wang et al. 2019](#); [Eilers et al. 2020](#)). These quasars are selected to be bright in both the rest-frame UV (AB magnitude $J \leq 19.8$ for

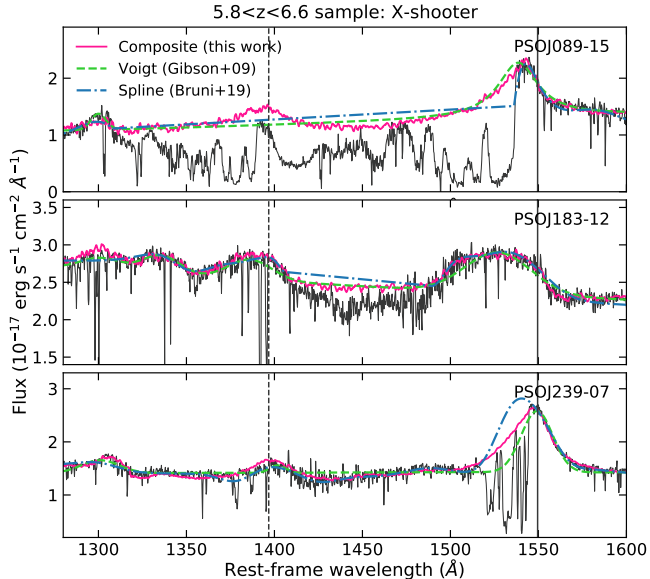


Figure 2. Example of three BAL quasars from the $5.8 < z < 6.6$ sample considered in this work. We show the comparison between our estimate of the intrinsic quasar emission, based on composite template spectra (Sect. 3.1), with the quasar emission model by Gibson et al. (2009) and the spline model by Bruni et al. (2019). Vertical solid and dashed lines refer to the rest-frame wavelength of C IV and Si IV, respectively.

$z < 6.0$ sources and $J \leq 20.0$ for quasars at $z \geq 6.0$) and in the rest-frame optical, being all detected by WISE in the W1($3.4\mu\text{m}$) and W2($4.6\mu\text{m}$) bands, and represent the brightest quasars that have been discovered at the time. Further details about the selection of XQR-30 quasars, data reduction of the X-shooter spectra, and the target list are given in (Bischetti et al. 2022, D’Odorico et al. in prep.). This sample benefits from deep X-shooter observations (SNR $\gtrsim 25$ per 50 km s^{-1} pixel in the rest-frame spectral range $1600\text{--}1700 \text{ \AA}$), and robust, Mg II-based black hole masses (Lai et al. 2022, Mazzucchelli et al., in prep.). A systematic search and characterization of C IV BAL outflows in XQR-30 was performed in Bischetti et al. (2022), based on the same approach used in this work (Sect. 3). Although X-shooter spectra of similar quality (SNR $\gtrsim 10$) exist to date for several luminous quasars at $5.0 < z < 5.4$, we do not consider them in this work as they have been mostly selected for studies of intervening absorbers and are therefore biased against the presence of BAL features (Becker et al. 2019).

3. IDENTIFICATION OF BAL QUASARS

3.1. Reconstruction of quasar continuum emission

To search for BAL absorption troughs, the first step is to model the intrinsic continuum emission in the rest-frame UV. A possible approach is to fit the spectra with

a quasar emission model accounting for continuum and line emission, and extrapolating this model to the spectral region affected by the BAL (Fig. 2). Models typically include a power-law component to reproduce the quasar continuum emission, and Voigt or gaussian profiles to account for emission lines (Gibson et al. 2009; Shen et al. 2011, 2019). Alternatively, more complex, non-physically motivated functions such as splines are sometimes used, as they can be more flexible in reproducing a variety of quasar spectra (e.g. Bruni et al. 2019). Both approaches require that a sufficiently large portion of the quasar spectrum is free from both absorption and emission lines, allowing to anchor the fit. However, this condition is often unsatisfied in the spectral region between Ly- α and C IV, resulting in large uncertainties (Fig. 2). In addition, both methods are largely dependent on the regions of the spectrum that are masked prior to fitting, especially in those cases where BAL features cover a wide spectral range or affect emission line profiles.

These uncertainties can be minimised using composite templates built from observed quasar spectra. Quasar spectra can be combined via different techniques such as principal component analysis (Trump et al. 2006; Pâris et al. 2018; Guo & Martini 2019) or non-negative matrix factorisation (Allen et al. 2011). Here we build, for each quasar of the sample, a composite template based on a large number of SDSS quasar spectra classified as non-BAL in Gibson et al. (2009), each matching within $\pm 20\%$ its color and the equivalent width (EW) of the C IV line (Shen et al. 2011). Given the anti-correlation between the EW of C IV and its blueshift with respect to the quasar redshift due to outflowing gas motions (Coatman et al. 2017; Vietri et al. 2018), the latter criterion allows us to reproduce all levels of asymmetry in the C IV line profile. A similar approach was recently adopted by Wang et al. (2018, 2021a), who created composite templates based on matching C IV blueshift of two $z > 7$ BAL quasars. The C IV EW or the blueshift criteria should in principle produce similar composite templates. However, SDSS quasar redshifts rely on automatic fitting procedures based on a limited spectral coverage, and are therefore affected by uncertainties on the C IV blueshift that can reach thousands of km s^{-1} , leading to an inaccurate selection of the quasar spectra contributing to the template. We find that a better spectrum-template agreement can be achieved by using the C IV EW during the selection of the quasar spectra.

Concerning the quasar colours, we consider the $F(1700\text{\AA})/F(2100\text{\AA})$ flux ratio to reproduce the continuum slope redwards of C IV, and the $F(1290\text{\AA})/F(1700\text{\AA})$ flux ratio, to account for a change

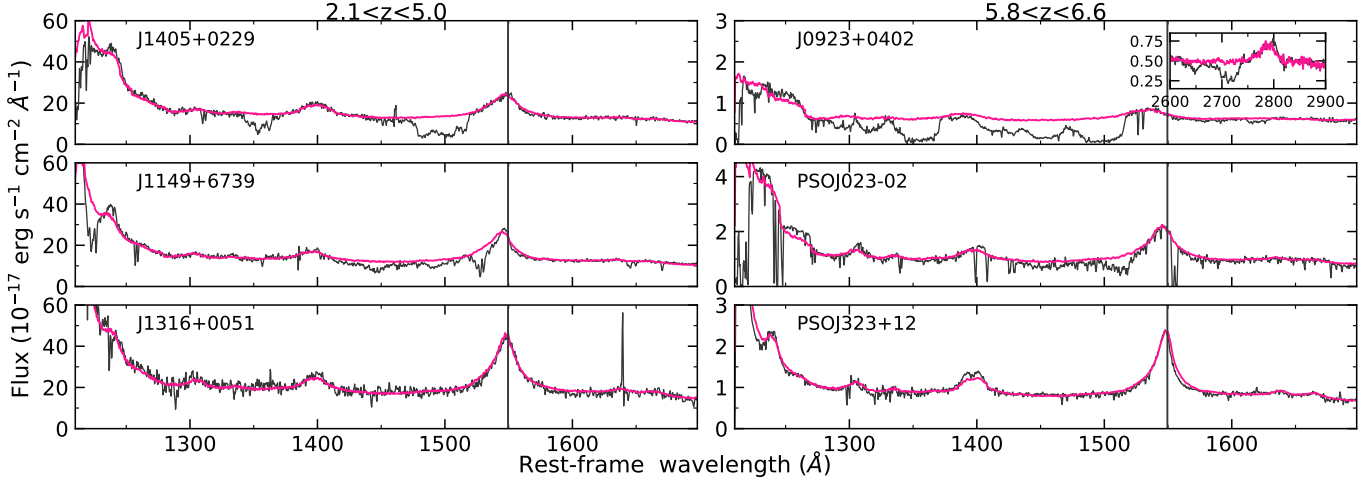


Figure 3. Examples of BAL (top and middle) and non-BAL (bottom) quasar spectra, randomly selected from our sample and binned to 50 km s^{-1} (black curves). Left(right) column shows SDSS(X-shooter) spectra. In the case of J0923+0402 ($z = 6.626$), the inset displays the spectral region close to Mg II affected by BAL features. Composite templates, used to estimate the intrinsic quasar emission, are shown by the magenta curve (Sect. 3.1). Vertical lines indicate the rest-frame wavelength of C IV.

in the continuum slope as observed in red quasar spectra (e.g. Trump et al. 2006; Shen et al. 2019). We calculate $F(1700\text{\AA})$ and $F(2100\text{\AA})$ as median flux values over 100 \AA and $F(1290\text{\AA})$ over 30 \AA in the rest-frame. The underlying assumption is that the observed and intrinsic continuum emission do not differ around 1290 \AA that is the bluest spectral region, redward of Ly- α , free from strong emission lines. In fact, Ly- α forest absorption complicates our measure of the $\lambda < 1216 \text{ \AA}$ quasar continuum, owing to the absorption becoming stronger with increasing redshift. In the case that BAL absorption troughs affect the spectral region close to 1290 \AA , our approach would provide a lower limit on the intrinsic quasar continuum emission and on the absorption BI (Sect. 2).

Starting from the total Shen et al. (2011) catalogue of 11800 SDSS quasars in the redshift range $2.13 < z < 3.20$, for which SDSS spectroscopy probes the $1216 - 2100 \text{ \AA}$ wavelength range, the composite template spectrum is built as the median of a hundred randomly selected, non-BAL (Gibson et al. 2009; Shen et al. 2011) quasar spectra. The above number is a trade-off between using stringent selection criteria and ensuring that the composite template is not affected by individual quasar spectra. The composite template is normalised to the median flux value of the quasar spectrum in the rest-frame $1650-1750 \text{ \AA}$ spectral interval, avoiding prominent emission lines and strong telluric absorption for the redshift interval covered by our sample (Smette et al. 2015). Figure 2 shows that the above approach provides us with (i) a solid reconstruction of the C IV profile even when affected by strong absorption features, (ii) a reasonable estimate of the quasar

emission blueward of C IV also in the most absorbed spectra, (iii) a conservative estimate of the continuum emission, typically lower or similar to the continuum reproduced by the Gibson et al. (2009), Bruni et al. (2019) models. Figure 3 shows examples of the SDSS and X-shooter spectra for the quasars belonging to the $2.1 < z < 5.0$ and $5.8 < z < 6.6$ samples, respectively. The X-shooter spectra and composite templates for the remaining $5.8 < z < 6.6$ quasars are shown in Fig. 11. Normalised spectra are obtained by dividing each spectrum by its matched composite template.

3.2. Characterisation of BAL troughs

The standard indicator used to identify absorption features in quasar spectra due to BAL outflows is the balnicity index (BI), firstly introduced by Weymann et al. (1991), which is a modified equivalent width of the BAL absorption and is more robust against false BAL quasar identifications than other indicators such as the AI (Knigge et al. 2008). Here we adopt the balnicity index definition by (Gibson et al. 2009):

$$BI_0 = \int_0^{v_{\text{lim}}} \left(1 - \frac{f(v)}{0.9} \right) C dv \quad (1)$$

where $f(v)$ is the normalised spectrum, $C = 1$ if $f(v) < 0.9$ for contiguous troughs of $> 2,000 \text{ km s}^{-1}$, $C = 0$ otherwise. We search the normalised spectra for BAL features in the region between Ly- α and C IV, that is corresponding to $v_{\text{lim}} \sim 64,000 \text{ km s}^{-1}$ for C IV BAL outflows, $\sim 35,000 \text{ km s}^{-1}$ for Si IV and $\sim 6,000 \text{ km s}^{-1}$ for N V, respectively. We do not extend the search to smaller wavelengths due to the stronger intergalactic medium absorption blueward of Ly- α with increasing

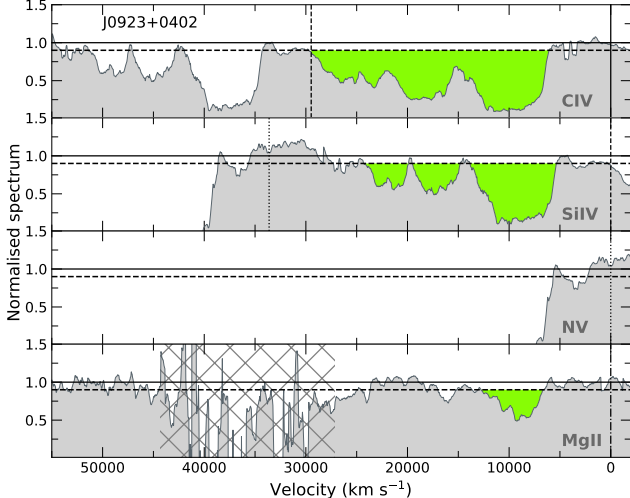


Figure 4. Example of normalised spectrum for BAL quasar J0923+0402 at $z = 6.626$, smoothed to 500 km s^{-1} . The velocity axis in each panel is relative to the rest-frame wavelength of the ionic species indicated by the label. Vertical solid, dashed, dotted and dashed-dotted lines indicate the velocity associated with C IV, Si IV, N V and Mg II emission lines, respectively. The solid(dashed) horizontal line represents a flux level of 1.0(0.9). BAL troughs, corresponding to a flux level < 0.9 (Eq. 1), are highlighted as green shaded areas. The hatched area indicates the spectral region affected by strong telluric features.

redshift, preventing us from a homogeneous BAL identification at different epochs. We identify the minimum (v_{\min}) and maximum (v_{\max}) BAL velocity for a given transition, as the lowest and highest velocity for which $C = 1$ in Eq. 1, respectively. Previous studies were typically limited to $v_{\lim} = 25,000 \text{ km s}^{-1}$ (Trump et al. 2006; Gibson et al. 2009; Guo & Martini 2019), to avoid discriminating between BAL outflows associated with C IV and Si IV ions. Here we exploit the fact that the C IV optical depth is usually similar or larger than the Si IV depth in BAL quasars (Dunn et al. 2012). This allows us to use the velocity range of the C IV BAL troughs to identify absorption associated with Si IV (Fig. 4, see also Wang et al. 2018; Bruni et al. 2019). This implies that absorption features blueward of Si IV are due to a low velocity Si IV BAL if a C IV BAL with similar velocity is observed. Otherwise, these features are considered to be produced by a high-velocity ($v_{\max} \gtrsim 30,000 \text{ km s}^{-1}$) C IV BAL (see also Rodríguez Hidalgo et al. 2020). We similarly assume that the C IV optical depth is larger than those of Mg II and N V and apply the methodology above to identify Mg II and BAL features. We measure the BAL width, defined as $w_{\max} = v_{\max} - v_{\min}$. The distributions of BI_0 , v_{\min} and v_{\max} for the C IV BAL quasars identified in our sample are shown in Fig. 2 of Bischetti et al. (2022), and values for individual quasars

Table 1. Si IV and N V BAL parameters

Name	Species	BI_0	v_{\min}	v_{\max}
(1)	(2)	(3)	(4)	(5)
PSOJ009-10	Si IV	2,880	33,080	38,360
PSOJ065+01	Si IV	660	17,240	27,190
PSOJ089-15	Si IV	8,150	2,280	28,040
	N V	2,280	2,270	5,870
J0923+0402	Si IV	7,970	6,110	24,330
PSOJ217-07	Si IV	440	30,460	35,000
PSOJ231-20	N V	630	560	2,640
PSOJ239-07	Si IV	230	830	3,360
	N V	1,810	820	5,720
J2211-3206	Si IV	3,420	9,550	19,120
J2250-5015	Si IV	1,320	29,460	37,540

NOTE—1) quasar ID, (2) Ionic species of the BAL, (3-5) balnicity index, minimum and maximum velocity of the Si IV BAL outflows, in units of km s^{-1} . Positive v_{\min} and v_{\max} values indicate blue-shifted absorption.

at $5.8 < z < 6.6$ are listed in their Table E1. The median uncertainties on BI_0 , v_{\min} , v_{\max} , and w_{\max} are 310, 200, 380, and 340 km s^{-1} , respectively (68% confidence level). These have been computed in Bischetti et al. (2022), taking into account the uncertainties on either the slope and normalisation of the composite template spectra.

3.3. Non-C IV BALs in the XQR-30 sample

Of the 14 quasars at $5.8 < z < 6.6$ hosting a C IV BAL outflow (Bischetti et al. 2022), eight also show a BAL system associated with the Si IV ion (namely PSOJ009-10, PSOJ065+01, PSOJ089-15, J0923+0402, PSOJ217-07, PSOJ239-07, J2211-3206, J2250-5015), three show a N V BAL (namely PSOJ089-15, PSOJ231-20, PSOJ239-07), and one (J0923+0402) shows a Mg II BAL. Figure 4 shows as an example the normalised spectrum of quasar J0923+0402 at $z \sim 6.6$, for which we identify strong BAL systems associated with C IV, Si IV, and Mg II ions. The C IV BAL is characterised by a $BI_0(\text{C IV}) = 15,370 \text{ km s}^{-1}$ and extends between $v_{\min}(\text{C IV}) = 6,090 \text{ km s}^{-1}$ and $v_{\max}(\text{C IV}) = 29,500 \text{ km s}^{-1}$ (Bischetti et al. 2022). We identify a Si IV BAL spanning a similar velocity range, with $BI_0(\text{Si IV}) = 7,390 \text{ km s}^{-1}$, and a less prominent Mg II BAL with $BI_0(\text{Mg II}) = 2,340 \text{ km s}^{-1}$. We cannot assess the presence of a N V BAL in this

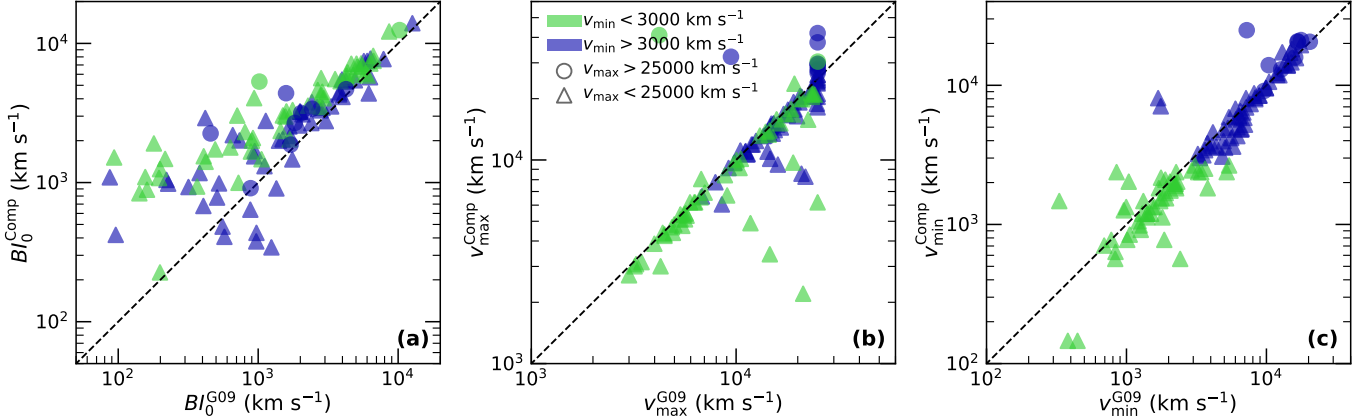


Figure 5. Comparison between the C IV BAL properties measured with our composite template method (Sect. 3.1) and in the analysis by Gibson et al. (2009) for the quasars in the $2.1 < z < 5.0$ sample. (a) balnicity index computed as in Eq. 1, (b) maximum velocity and (c) minimum velocity of the BAL outflows. In all panels, the dashed line indicates a 1:1 relation.

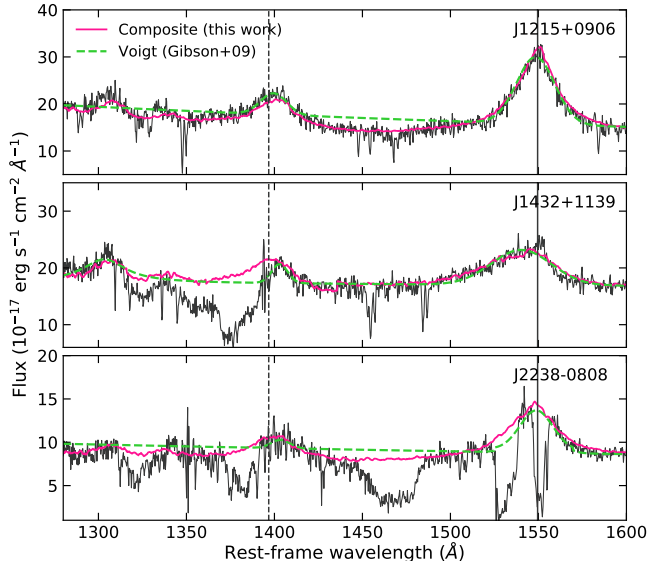


Figure 6. Example of SDSS spectra for three BAL quasars from the $2.1 < z < 5.0$ sample. We show the comparison between our reconstruction of the intrinsic quasar emission, based on composite template spectra (Sect. 3.1), and the prescription by Gibson et al. (2009). Different recipes can lead to a different BAL/no-BAL classification (J1215+0906 and J1432+1139), and to different BI_0 (J2238-0808), see Sect. 3.4 for details. Vertical solid and dashed lines refer to the rest-frame wavelength of C IV and Si IV, respectively.

quasar, because of almost no transmitted flux blueward of Ly- α .

We thus classify 12 quasars as HiBALS, and quasar J0923+0402 ($z \simeq 6.63$) as a LoBAL. In the case of PSOJ189-15 ($z \simeq 5.97$), strong telluric contamination affecting the spectral region blueward of Mg II does not allow us to validate/rule out the presence of a Mg II BAL. Our results increases by a factor of about four

the number of Si IV BAL quasars identified at $z \gtrsim 6$ (Wang et al. 2018, 2021a). The presence of a Si IV BAL in J2211-3206 ($z = 6.33$) was previously suggested by Chehade et al. (2018). A few hints of Mg II absorption in $z \gtrsim 6$ quasars have been reported so far (e.g. Maiolino et al. 2004; Wang et al. 2021a).

The BAL parameters measured for the Si IV and N V BAL outflows are listed in Table 1, and their residual spectra are shown in Fig. 12. The Si IV BAL features are characterised by $BI_0 \sim 200 - 8,100 \text{ km s}^{-1}$, which are typically smaller (10-60%) than those measured in C IV, consistently with what has been found for SDSS quasars (Gibson et al. 2009). The only exception is PSOJ009-10, for which $BI_0(\text{C IV}) = 1,110 \text{ km s}^{-1}$ (Bischetti et al. 2022) and $BI_0(\text{Si IV}) = 2,880 \text{ km s}^{-1}$. However, this quasar shows a very red spectrum with almost no Ly- α and N V emission, overfitted by the composite template at $\lambda < 1270 \text{ \AA}$ (Fig. 11). This suggests strong absorption, consistent with the presence of a Si IV BAL outflow, whose properties are nevertheless highly uncertain. For the N V BALs, we measure $BI_0 \sim 600 - 2,300 \text{ km s}^{-1}$.

3.4. Re-analysis of SDSS quasar spectra

Given that the $2.1 < z < 5.0$ quasars in our sample did not benefit from a homogeneous identification and characterisation of BAL outflows from the literature (Sect. 2.2), we have re-analysed their spectra following the approach described in Sect. 3. In Fig. 5 we compare our results with those by Gibson et al. (2009), who provided BI_0 , v_{\min} and v_{\max} for the 1317 SDSS DR5 quasars in our sample (Schneider et al. 2007). We recover 162 out of the 207 BAL quasars identified by Gibson et al. (2009). The remaining quasars, classified as non-BAL quasars in our analysis, have only very weak BAL absorption in Gibson et al. (2009) (all but 5 have

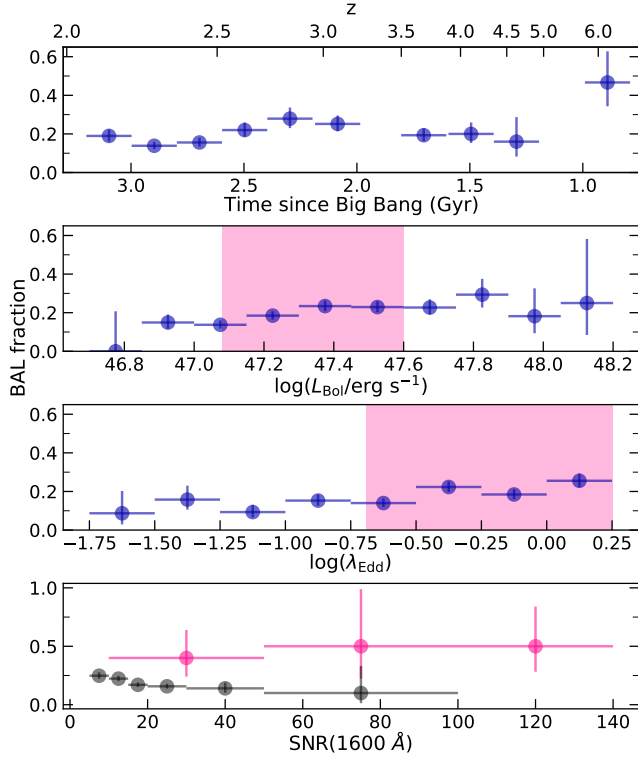


Figure 7. BAL fraction as a function of different physical quantities. Top: cosmic time, from 0.8 to 3.2 Gyr from the Big Bang, in bins of ~ 200 Myr. Top axis indicate the corresponding redshift interval. Second from top: quasar bolometric luminosity, estimated from the rest-frame optical via bolometric correction. Second from bottom: accretion rate. Shaded areas indicate the range of L_{Bol} and λ_{Edd} of the $5.8 < z < 6.6$ sample (Sect. 2.3, Mazzucchelli et al. in prep.). Bottom: median SNR of the quasar spectra at 1600 \AA (Sect. 4). Black(magenta) dots refer the $2.1 < z < 5.0$ ($5.8 < z < 6.6$) sample. In each panel, horizontal bars indicate the bins in which BAL fractions have been calculated, while vertical bars show Poissonian uncertainties at a 90% confidence level for each bin.

$BI_0 < 500 \text{ km s}^{-1}$), likely owing to the flat continuum emission in the C IV-Si IV spectral region not well reproduced by the reddened power-law continuum model used by Gibson et al. (2009), introducing a small systematic on the true continuum level. One example is shown in Fig. 6 top panel for quasar SDSSJ1215+0906 ($z = 2.72$), previously classified as a BAL quasar with $BI_0 \simeq 120 \text{ km s}^{-1}$ by Gibson et al. (2009), which we instead identify as a non-BAL. In addition, small differences between the DR5 and DR7 spectra can easily produce BI_0 variations of a few hundred km s^{-1} (e.g. Byun et al. 2022; Vietri et al. 2022). On the other hand, we identify 39 new BAL quasars that were classified as non-BALs by Gibson et al. (2009). One example is SDSS quasar J1432+1139 ($z = 2.99$, Fig. 6 middle

panel), showing high-velocity C IV BAL features with $v_{\text{min}} \sim 29,000 \text{ km s}^{-1}$, that is outside the spectral range investigated by Gibson et al. (2009). When comparing the properties of the BAL quasars identified in both our work and Gibson et al. (2009), we find on average no systematic difference in BI_0 , with a significant scatter at $BI_0 \lesssim 1,000 \text{ km s}^{-1}$ (Fig. 5a). We note that we typically measure larger BI_0 in those cases in which the absorption has $v_{\text{min}} < 3,000 \text{ km s}^{-1}$ and thus affects the blue side of the C IV line, as it can be seen for SDSS J2238-0808 ($z=3.17$) in Fig. 6 bottom panel. This is due to the fact that our composite templates better reproduce the asymmetric C IV profiles, typically showing a more prominent blue wing due to ionised outflows, than the Voigt profiles in Gibson et al. (2009). We also recover higher BI for those quasars in which the BAL absorption reaches v_{max} higher than $25,000 \text{ km s}^{-1}$.

The majority of the C IV BAL outflows show v_{max} and v_{min} velocities similar to those measured by Gibson et al. (2009). In a few cases, we measure lower v_{max} because of the different continuum treatments, and we identify a subsample of BAL quasars with extremely fast BAL outflows ($v_{\text{max}} \sim 25000 - 40000 \text{ km s}^{-1}$, Fig. 5b), missed by Gibson et al. (2009). This is consistent with the results of Bruni et al. (2019); Rodríguez Hidalgo et al. (2020), who reported the presence of BAL outflows reaching velocities of 10–15% of the light speed in a small fraction of SDSS quasars at $z \sim 2 - 4$. In the case of absorption with $v_{\text{min}} < 3,000 \text{ km s}^{-1}$ (Fig. 5c), we typically measure v_{min} lower by a factor of about two with respect to Gibson et al. (2009) estimates, likely because the Voigt profiles employed in their modelling underestimate the intrinsic emission of the C IV blue wing (Fig. 6 bottom).

4. BAL QUASAR FRACTION

Figure 7 shows the evolution of the BAL quasar fraction across a cosmic time interval of about 2.3 Gyr, corresponding to the redshift range $2.1 < z < 6.6$ probed by our sample. We find the BAL fraction to be almost constant at $z \lesssim 4.5$ with a median value of $\sim 20\%$. This is in agreement with the fraction calculated for the $2.1 < z < 5.0$ sample in Bischetti et al. (2022) and with previous studies focusing on rest-frame optical bright quasars with similar redshift (Dai et al. 2008; Maddox et al. 2008). The oscillations around this value are likely due to the SDSS quasar selection systematics, affecting differently BAL and non-BAL quasars as a function of redshift, that are minimised but not totally removed by our sample selection (Sect. 2.1). Indeed, BAL quasars are expected to be less-efficiently selected than non-BALs at $z < 2.5$, more efficiently selected at

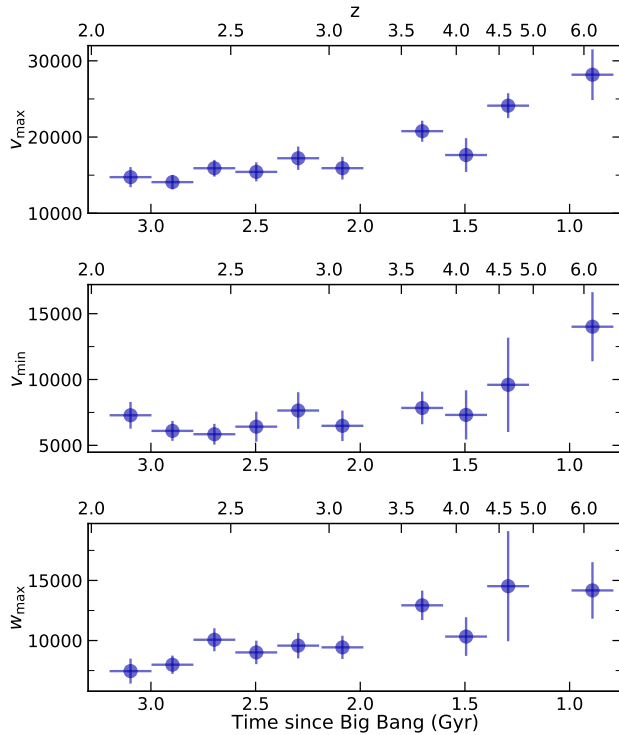


Figure 8. Maximum velocity (top), minimum velocity (middle) and maximum width (bottom) of the C IV BAL outflows, in units of km s^{-1} , as a function of cosmic time. Top axes indicate the sampled redshift interval. Horizontal bars indicate the individual time bins of ~ 200 Myr in which the average BAL velocity has been calculated. Vertical bars indicate the standard error on the average value for each time bin.

$2.6 < z < 3.1$, while no significant difference in the selection efficiency is predicted for $3.1 < z < 3.5$ (Reichard et al. 2003). The BAL fraction is instead significantly higher at $z \gtrsim 6$, by a factor of about 2.5 (Bischetti et al. 2022). The lack of data at $z \sim 5$ does not allow us to assess whether the decrease in the BAL fraction at $z < 6$ is smooth, consistently with secular evolution of the BH accretion properties, or whether it rapidly drops after $z \sim 6$, due to efficient BH feedback at early epochs (see Sect. 6.1).

To investigate whether the BAL fraction depends on nuclear properties of the quasar, Figure 7 also shows the BAL fraction as a function of L_{Bol} and λ_{Edd} . A common approach to derive L_{Bol} of high redshift quasars consists in applying a bolometric correction (Richards et al. 2006; Runnoe et al. 2012) to the monochromatic luminosity of the rest-frame UV continuum (e.g. Mazzucchelli et al. 2017). Bischetti et al. (2022) found no significant increase in the BAL fraction of $z \sim 2-4$ quasars in the luminosity range $\log(L_{\text{Bol}}/\text{erg s}^{-1}) \simeq 46.5 - 48$, even after correcting the UV-continuum level for the

BAL absorption. However, because BAL quasars typically show redder slopes of the UV continuum (Trump et al. 2006; Gibson et al. 2009; Allen et al. 2011) also in the high-luminosity regime spanned by our sample, using a common bolometric correction may result in an underestimate of L_{Bol} in BAL quasars. We do not correct the continuum luminosity for dust extinction because of the limited spectral range covered by the SDSS spectra, resulting in substantial degeneracy between the UV continuum shape and the magnitude of intrinsic reddening (e.g. Gibson et al. 2009). Also, one would need to assume an extinction law and possibly also its evolution with redshift (e.g. Gallerani et al. 2010), increasing the uncertainties on L_{Bol} . Instead, because all quasars in our sample are detected in the rest-frame optical, we derive an independent estimate of L_{Bol} by applying the $\sim 5100 \text{ \AA}$ bolometric correction by Runnoe et al. (2012) to the 2MASS H(K) fluxes for the $2.13 < z < 3.2$ ($3.6 < z < 5.8$) subgroups in our low- z sample, and to the WISE W1 fluxes for the high- z sample. The optical-based and UV-based bolometric luminosities are consistent for non-BAL quasars, while the optical-based L_{Bol} are typically higher by a factor of two for BAL quasars. Figure 7 shows a mild increase of the BAL fraction with the optical-based L_{Bol} , from $\sim 20\%$ to 25% . A clearer trend is observed between the BAL fraction and λ_{Edd} , with a factor of two increase in the BAL fraction for $\log\lambda_{\text{Edd}} \in [-1.7, 0.2]$ up to $\sim 25\%$ although we caution that most of the BH masses for our $2.1 < z < 5.0$ are based on the C IV line width, which can be significantly altered by the presence of BAL absorption with velocities of a few thousands km s^{-1} . This is consistent with the results from previous studies focusing on luminous quasars at $z \sim 2-4$ (Dai et al. 2008; Bruni et al. 2019). Nevertheless, neither the L_{Bol} nor the λ_{Edd} trends can account for the $\sim 47\%$ BAL fraction measured for the $5.8 < z < 6.6$ sample (median $\log(L_{\text{Bol}}/\text{erg s}^{-1}) = 47.3$, median $\lambda_{\text{Edd}} = -0.10$, Mazzucchelli et al. in prep.).

Finally, we investigate the dependence of the BAL fraction on the SNR of the quasar spectra. To this purpose, we homogeneously compute the spectral noise for our quasar sample as the median rms in the rest-frame interval $1650-1750 \text{ \AA}$ for a 70 km s^{-1} spectral pixel (Sect. 3.1). Figure 7 (bottom) shows no trend of the BAL with SNR for the $5.8 < z < 6.6$ sample, while it decreases with increasing SNR for the $2.1 < z < 5.0$ sample. This is likely due to the combination of (i) a similar rms sensitivity for the spectra, and (ii) bluer continuum slopes, translating into higher SNR for the non-BAL quasars in our sample. Previous studies of BAL quasars in SDSS reported no or little increasing

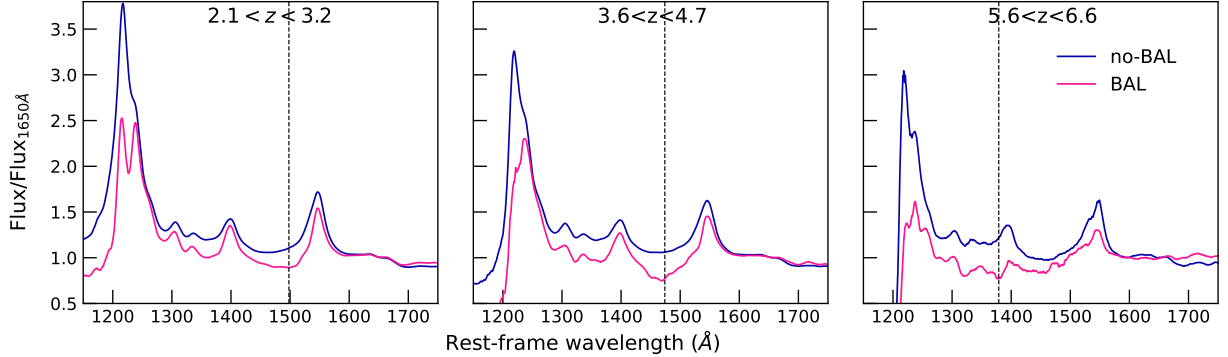


Figure 9. Composite template spectra of the BAL and non BAL quasars in our sample, in three bins of increasing redshift (from left to right). For each panel, composite spectra have been normalised to the median continuum flux at 1600–1700 Å. The vertical line indicates the rest-frame wavelength corresponding to the maximum depth of the C IV absorption, showing a shift toward lower wavelengths with increasing redshift. In the right panel, we consider only quasars with prominent BAL features ($BI_0 > 1,000 \text{ km s}^{-1}$, Bischetti et al. 2022).

trend (a few %) of the BAL fraction with SNR, for a similar range of $\text{SNR} = 10 - 50$ (Gibson et al. 2009; Allen et al. 2011), likely reflecting the mild trend with L_{Bol} , due to the wider (by about one order of magnitude) quasar luminosity range sampled by these works. We conclude that the increasing trend of the BAL fraction at $z \gtrsim 6$ is a genuine cosmic evolution and does not depend either on trends with nuclear properties or on the SNR of the spectra.

5. KINEMATIC PROPERTIES OF BAL OUTFLOWS

Here we investigate the evolution of the BAL kinematics across cosmic time, as traced by v_{max} , v_{min} and w_{max} (Sect. 3.2). Top panel of Fig. 8 shows that the maximum velocity of BAL outflows significantly increases by a factor of about two between $z \sim 2 - 3$ ($v_{\text{max}} \sim 15,000 \text{ km s}^{-1}$) and $z \sim 6$ ($v_{\text{max}} \sim 30,000 \text{ km s}^{-1}$). A similar trend is observed also for the minimum BAL velocity, reaching a typical value of $v_{\text{min}} \sim 15,000$ at $z \sim 6$. An increased fraction of BAL quasars with $v_{\text{max}} \gtrsim 30,000 \text{ km s}^{-1}$ at $z \sim 4 - 4.5$ was recently suggested by Rodríguez Hidalgo et al. (2020). Because of the larger increase of v_{max} with respect to v_{min} as a function of redshift, the width of the BAL features also increases between $z \sim 2 - 3$ ($9,000 \text{ km s}^{-1}$) and $z \sim 6$ ($15,000 \text{ km s}^{-1}$). Figure 9 shows that, because of the combination of the above trends, the composite spectrum of BAL quasars is differently affected by absorption features in three intervals of increasing redshift. The lowest redshift bin ($2.1 < z < 3.2$) shows that the absorption typically affects the blue side of C IV and the deepest absorption is located at 1,500 Å (i.e. blueshifted by $\sim 9,000 \text{ km s}^{-1}$). At intermediate redshift ($3.6 < z < 5.0$) the C IV wing is still partially altered by the absorption, which affects the whole spectral range between C IV and Si

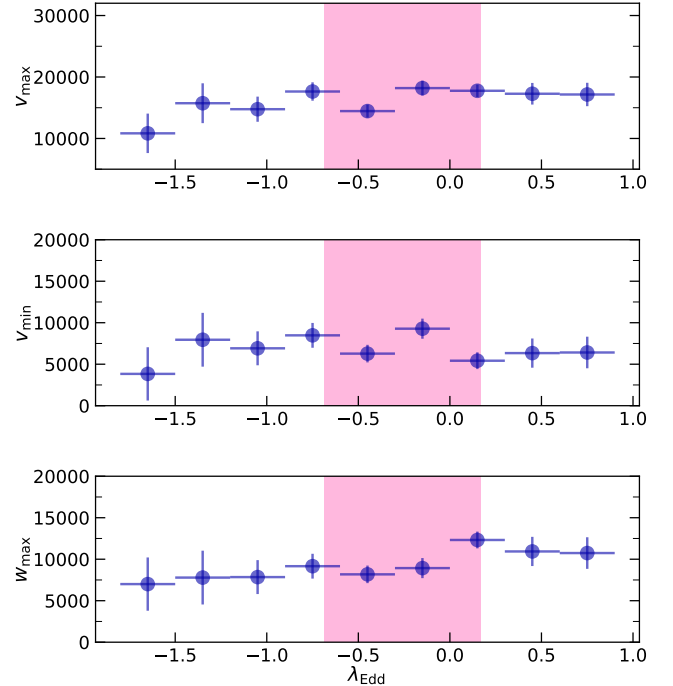


Figure 10. Maximum velocity (top), minimum velocity (middle) and maximum width (bottom) in units of km s^{-1} , as a function of λ_{Edd} for the C IV BAL outflows in our quasar sample. Horizontal bars indicate the accretion rate bins in which the average BAL velocity has been calculated. Vertical bars indicate the standard error on the average value for each bin. The shaded area indicates the range of λ_{Edd} of the $5.8 < z < 6.6$ sample (Mazzucchelli et al. in prep.).

IV. The deepest absorption is blueshifted by $\sim 15,000 \text{ km s}^{-1}$. In the highest redshift interval ($5.8 < z < 6.6$) the absorption is even broader and extends blueward of Si IV, down to $\sim 1,300 \text{ Å}$. The deepest absorption is blueshifted by $\sim 33,000 \text{ km s}^{-1}$. We note that, owing to the very broad distributions of v_{max} , v_{min} in combina-

tion with the small sample size in this high-redshift bin, we include in Fig. 9 only BALs with the most prominent features ($BI_0 > 1,000 \text{ km s}^{-1}$, Bischetti et al. 2022). These results, together with the higher BAL fraction observed in quasars at $5.8 < z < 6.6$, suggest an evolution of the BAL properties with cosmic time.

To test whether there is a dependence of the BAL kinematics on nuclear quasar properties, we show in Figure 10 the relations between v_{\max} , v_{\min} and w_{\max} , as a function of the BH accretion rate. We find no evident increase of either v_{\max} and v_{\min} with increasing λ_{Edd} over about two orders of magnitude, with an almost constant $v_{\max} \sim 15,000 - 17,000 \text{ km s}^{-1}$ and $v_{\min} \sim 5,000 - 7,000 \text{ km s}^{-1}$. There is a hint for a higher w_{\max} at high accretion rates, likely due to the lower v_{\min} observed in the three bins with the highest λ_{Edd} . Similarly, we observe no significant trend of the BAL kinematics with L_{Bol} , likely due to the limited luminosity range spanned by our sample. Indeed, no or only mild trends of increasing v_{\max} with L_{Bol} , λ_{Edd} were suggested by previous works studying BAL quasars in SDSS in a wider range of L_{Bol} (Ganguly et al. 2007; Gibson et al. 2009; Bruni et al. 2019). These results confirm that the trend of increasing v_{\min} , v_{\max} , and w_{\max} with redshift in our quasar sample cannot be explained by variations in the quasar nuclear properties, but rather points to an evolutionary effect.

6. DISCUSSION

6.1. Cosmic evolution of BAL outflow properties

In this work we have applied a homogeneous BAL identification method to a sample of 1935 $2.1 < z < 6.6$ quasars, which has allowed us to investigate self-consistently the evolution of the occurrence and kinematic properties of BAL outflows across ~ 3.2 Gyr. The sample includes luminous quasars (UV absolute magnitude ~ -27 , see Fig. 1), which have been selected to be luminous in the rest-frame optical to minimise the systematics on the BAL fraction at different redshifts (Sect. 2, see also Bischetti et al. 2022). Despite spanning about two orders of magnitude in terms of BH accretion rate, the bulk of the quasars in our samples are powered by efficiently-accreting BHs ($\log \lambda_{\text{Edd}} \sim -0.5$).

In this luminosity and BH accretion regime, we observe an evolution with redshift of the properties of BAL outflows. We find that the BAL fraction below $z \sim 4.5$ is almost constant and close to 20 – 25% (Fig. 7), while it significantly increases up to almost 50% at $z \sim 6$. The trend at $2.1 < z < 4.5$ is consistent with the results of previous studies focusing on rest-frame optical luminous quasar samples (Maddox et al. 2008; Dai et al. 2008, when considering the BI_0 criterion to iden-

tify BAL features), which reported a modest evolution of the BAL fraction with redshift. However, heavily-reddened broad-line quasars are expected to represent a high fraction of the bright quasar population at $z > 2$ (Banerji et al. 2015; Glikman et al. 2018), and may be missed by SDSS, from which our $2.1 < z < 4.5$ sample is drawn. Several recent surveys (e.g. Schindler et al. 2019; Boutsia et al. 2021; Grazian et al. 2022) have indeed shown that the SDSS selection of bright quasars at high redshift could possibly suffer from incompleteness by up to 30 – 40% at $z \sim 4$, and up to a factor of a few at $z \sim 5$ (Wolf et al. 2020; Onken et al. 2022), plausibly affecting also $z \sim 6$ quasars. In addition, our $5.8 < z < 6.6$ quasar sample is limited to $J \leq 19.8 - 20.0$ magnitudes and probes similar depths in the J and WISE bands (see Table ED1 in Bischetti et al. 2022). Accordingly, we may miss red BAL quasars at $z \sim 6$, detected by WISE but too faint in the rest-frame UV to match our selection (e.g. Kato et al. 2020). The BAL fractions we observe at $z \gtrsim 5$ may thus likely represent lower limits, implying BAL quasars to be much more common at early cosmic epochs.

By investigating the dependence of the BAL fraction on quasar nuclear properties, we can safely exclude that the large difference between the BAL fraction at $z \lesssim 4.5$ and $z \sim 6$ is due to differences in quasar luminosity and accretion rate. Instead, the higher BAL fraction at $z \sim 6$ can be explained either with wider angle outflows or as a result of longer blow-out phases of BH-driven outflows compared with $z \lesssim 4.5$ (Bischetti et al. 2022). A redshift evolution of the BAL geometry is indeed suggested by the fact that the velocity range spanned by the BAL troughs, as traced by w_{\max} , increases with redshift (Murray & Chiang 1998; Elvis 2000; Hall et al. 2002). Although linking w_{\max} to the velocity dispersion of the outflowing gas is not straightforward, as we mostly observe blends of outflowing gas components (e.g. Borguet et al. 2013), the increase of w_{\max} may be interpreted as stronger turbulence in the higher redshift BAL outflows. In a scenario of Chaotic Cold Accretion (CCA), gas turbulence on scales similar to those of BALs (~ 100 pc, Arav et al. 2018) is linked to the condensation and funnelling of the cold gas phase toward the BH, higher turbulence implying stronger inflows and, in turn, triggering more efficient phases of BH feedback (Gaspari et al. 2020).

We also find that the BAL velocity (either v_{\max} and v_{\min}) typically increases with redshift, suggesting that BAL outflows in the high- z Universe might be more easily accelerated than at later cosmic epochs. A viable explanation might be linked to the presence of dust mixed with the ionised gas in the BAL clouds,

which would significantly increase the radiation boost efficiency (Ishibashi et al. 2017; Costa et al. 2018) and therefore accelerate the BAL outflows to the observed extreme $v_{\max} \sim 20,000 - 50,000 \text{ km s}^{-1}$. Peculiar dust properties in the $5.8 < z < 6.6$ BAL quasar sample have been indeed suggested by Bischetti et al. (2022), who found that BAL quasars are systematically redder than non-BAL quasars. At later cosmic epochs, although BAL quasars are known to show relatively redder UV colours (Reichard et al. 2003; Trump et al. 2006; Gibson et al. 2009), no strong difference in the optical colours of BAL and non-BAL quasars is typically observed, at least in optically-bright sources (Dai et al. 2008; Bischetti et al. 2022).

Alternative scenarios that could explain the higher BAL velocities at early epochs might be related to different properties of BH accretion at different redshift. CCA toward the BH is expected to be favoured at higher redshift, because of a larger fraction of a clumpy cold gas phase in the quasar hosts, boosting BH-driven outflows to higher velocities (Gaspari & Sadowski 2017). Also, BALs at high redshift could be launched with higher velocities if BHs are spinning more rapidly than at later epochs. BH spins are indeed expected to decrease over cosmic time (King et al. 2008; Zubovas & King 2021). High BAL velocities have been more commonly found in sources with softer spectral energy distributions, that is lower X-ray to optical luminosity ratios, either from direct X-ray observations of low- z quasars (Laor & Brandt 2002) or using indirect tracers such as the EW of the He II $\lambda 1640 \text{ \AA}$ emission line in SDSS quasars, (Richards et al. 2011; Baskin et al. 2015; Rodríguez Hidalgo et al. 2020). For the highest redshift bins in which we observe the larger increase in v_{\max} , v_{\min} (see Fig. 8), very limited information about the X-ray properties exist. Indeed a total of a few tens of quasars have been targeted with sensitive observations at $z > 5$ to date, including only a few BAL quasars, some of which do exhibit the softest optical-to-X-ray slopes (Nanni et al. 2017; Vito et al. 2019; Wang et al. 2021b). The weakness of the He II emission line makes its detection very challenging at these redshifts (e.g. Shen et al. 2019). The characterisation of the He II emission in the $5.8 < z < 6.6$ sample, enabled by the high-SNR of the X-shooter spectra from the XQR-30 survey, will be presented by Bischetti et al. in preparation.

6.2. Impact of BAL outflows on BH and galaxy-evolution

The broad and often saturated BAL profiles associated with CIV hamper prevent us from an accurate measurement of the outflowing gas mass and, in turn, of the

energy injected by the outflow into the galaxy medium (Dunn et al. 2012; Borguet et al. 2013). Nevertheless, assuming similar outflow masses (Moe et al. 2009; Dunn et al. 2010), we can estimate that BAL quasars at $z \sim 6$ inject about 20 times more energy with respect to $z \sim 2 - 4$ quasars (Bischetti et al. 2022), as the outflow kinetic power linearly scales with the BAL fraction and with the square power of v_{\max} (Fiore et al. 2017). This result strongly points towards a phase of efficient BH feedback occurring at $z \sim 6$, as the energy injected by these BAL outflows will likely suppress gas accretion and slow down BH growth (e.g. Torrey et al. 2020). This likely represents the first observational evidence of what has been so far only predicted by cosmological simulations of the early assembly of bright quasars. BHs at the centre of bright quasars are indeed expected to grow exponentially at very high redshift ($z >> 6$), with accretion rates close to the Eddington limit or beyond (Inayoshi et al. 2016; Pezzulli et al. 2016), while around $z = 6$ BH growth is expected to significantly slow down because BH feedback has become strong enough to remove gas from the central galaxy regions and to prevent further accretion onto the BH (Costa et al. 2014; van der Vlugt & Costa 2019). In addition, BHs powering bright quasars at $z \sim 6$, with typical masses of $\sim 10^9 \text{ M}_\odot$ (Mazzucchelli et al. 2017; Shen et al. 2019; Farina et al. 2022), have been found to be typically overmassive by a factor of ~ 10 with respect to the mass of their host-galaxies, when compared to the BH mass vs galaxy dynamical mass relation observed in the low-redshift Universe (Gaspari et al. 2019; Pensabene et al. 2020; Neeleman et al. 2021). Preliminary measurements of the BH mass (based on the Mg II line, Mazzucchelli et al. in prep.) and of the dynamical mass (based on spatially-resolved C II $\lambda 158 \mu\text{m}$ observations, Bosman et al. in prep.) for the quasars in our $5.8 < z < 6.6$ sample confirm this result, indicating that BH growth must have dominated over the host-galaxy growth at $z >> 6$ and that a transition epoch during which BH growth decelerates must occur at $z \lesssim 6$, leading toward the symbiotic BH and galaxy growth (e.g. Lamastra et al. 2010; Zubovas & King 2021; Inayoshi et al. 2022). An early BH mass assembly in bright quasars occurring at $z > 6$ is also supported by the fact that the largest BH masses measured at $z \sim 6$ and at $z \sim 2$ only differ by a factor of a few (Trakhtenbrot 2021) and by the increase of the median BH accretion rate with redshift for a given quasar luminosity (Yang et al. 2021; Farina et al. 2022).

Although the above scenario points toward BH feedback as a likely driver of BH growth suppression, other physical processes might be also in place. The cosmic evolution of the BAL fraction is key to identify the

dominant mechanism responsible for slowing down BH growth. Indeed, a sharp decrease of the BAL fraction occurring between $z \sim 6$ and $z \sim 5$ would strongly point toward a phase of efficient BH feedback, which is expected to occur on a short timescale (few tens of Myrs (Negri & Volonteri 2017) and quickly remove gas from the central regions of the galaxy, thus dominating this transition (Zubovas & King 2013). Conversely, a smooth decrease of the BAL fraction from $z \sim 6$ to $z \sim 4$, would rather indicate that several processes may be at play in the transition, including a (less efficient) BH feedback and secular processes, such as a change in the merger rate or in the gas condensation rate, reducing the active phase duty cycle on a timescale of several hundreds of Myrs (Gaspari et al. 2019; O’Leary et al. 2021). To discriminate between these competing scenarios, a crucial step is to obtain a reliable measure of the evolution of the BAL fraction with redshift in representative samples, with a cosmic time sampling $< 100 - 200$ Myr. Currently, the sample presented in this work and, particularly, the lack of sources at $5 < z < 5.8$ do not allow us to accurately probe the high-redshift evolution of the BAL fraction between $z \sim 4.5$ and $z \sim 6$. New high quality spectroscopic observations of an absorption-unbiased sample of rest-frame optical bright quasars are necessary to fill this gap and test whether efficient BH feedback is the dominant mechanism leading to the symbiotic BH-galaxy growth phase.

On the other hand, it is unclear whether and on what timescales BAL outflows can affect the evolution of the host-galaxies of $z \sim 6$ quasars. Observations of BAL quasars at intermediate redshift report mass outflow rates up to several hundreds of M_{\odot}/yr (e.g. Fiore et al. 2017; Bruni et al. 2019), consistent with theoretical expectations from models of BH-driven outflows for an efficient feedback mechanism (Faucher-Giguère & Quataert 2012; Zubovas & King 2012) and outflow sizes based on photo-ionisation analysis that can reach kpc scales (Arav et al. 2018; Byun et al. 2022), suggesting that BAL outflows may also affect the physical properties of the galaxy medium and, in turn, the galaxy growth.

If the effect of BH feedback extends to kpc scales, a correlation with the star formation rate (SFR) would be expected, while conflicting results have been reported so far. Authors found either reduced (Farrah et al. 2012; Zhang et al. 2014) or enhanced SFR (Wethers et al. 2020), or no significant difference (Cao Orjales et al. 2012; Laha et al. 2021; Pitchford et al. 2016) in BAL and non-BAL quasars. Observations of the sub-millimetre dust continuum emission exist for several tens of $z \sim 6$ quasars (e.g. Venemans et al. 2018; Decarli et al. 2018; Carniani et al. 2019), and large SFR of a

few hundreds up to a few thousands of M_{\odot}/yr are found. However, these SFR measurements typically suffer from large uncertainties, up to one order of magnitude, due to the poor (or lack of) sampling of the peak of the sub-millimetre spectral energy distribution (e.g. Wang et al. 2019; Tripodi et al. 2022). In addition, disentangling SF and quasar contributions to dust heating requires a treatment of radiative transfer (Bianchi 2008; Duras et al. 2017; Di Mascia et al. 2021). High-frequency (Bands 8 and 9) ALMA observations and JWST observations will be fundamental to accurately measure the SFR in the high-redshift quasar hosts. This will allow us to test the connection between BH feedback due to BAL outflows and the host-galaxy SFR at $z \sim 6$.

A correlation is also expected between the strength of BH feedback and the cooling rate of the hot and warm gas phases in the quasar host galaxies, due to heating and turbulence injection into the ISM (e.g. Gaspari 2015). JWST will also allow us to measure the cooling rates of the warm gas, e.g. using the [OIII] $\lambda 4363\text{\AA}/(\lambda 5007\text{\AA} + \lambda 4959\text{\AA})$ diagnostic for the gas temperature, and to investigate a possible suppression of cooling rates in BAL quasars out to $z \gtrsim 6$.

7. CONCLUSION

In this work we analyse a sample of 1935 luminous (bolometric luminosity $L_{\text{bol}} \gtrsim 10^{47} \text{ erg s}^{-1}$) quasars at $z = 2.1 - 6.6$, drawn from the Sloan Digital Sky Survey (Shen et al. 2011) and from the X-shooter legacy survey of Quasars at Reionisation (Bischetti et al. 2022, see also D’Odorico et al. in prep. for a complete description of the survey), to investigate the evolution with cosmic time of the BAL fraction and of the kinematics of BH-driven outflows, as traced by BAL features. Targeting rest-frame optical bright quasars allows us to reduce biases due to quasar selection criteria (Sect. 2.1).

We apply a homogeneous BAL identification method to the total sample, based on composite template spectra to estimate the intrinsic quasar continuum and line emission (Sect. 3). This approach allows us to well reproduce the spectral region between Ly- α and C IV for a variety of BAL shapes, without any assumptions on the continuum shapes, nor on the spectral regions in which absorption might occur. At the same time, it takes into account the asymmetry often observed in the C IV profile due to the presence of outflowing gas.

We find that the BAL fraction is about 20% and does not vary strongly across this redshift range, in agreement with previous works (Dai et al. 2008; Maddox et al. 2008), while it increases to almost 50% at $z \sim 6$ (Bischetti et al. 2022). We also investigate the dependence of the BAL fraction with quasar nuclear properties such

as L_{Bol} , λ_{Edd} , and we observe only weak correlations given the ranges of luminosity and accretion rate probed by our sample, in agreement with previous results for SDSS quasars (e.g. [Gibson et al. 2009](#); [Bruni et al. 2019](#)). These trends cannot account for the increase in the BAL fraction observed in the $5.8 < z < 6.5$ sample (Sect. 4).

We also observe a redshift evolution of the BAL kinematics. Both v_{max} and v_{min} increases at $z \gtrsim 4$, the typical BAL velocities at $z \sim 6$ being a factor of 2-3 higher than what observed at $z < 4$ (Sect. 5). The width of the BAL features also likely increases at $z \gtrsim 4$. These trends suggest a possible evolution of the BAL geometry and are consistent with BALs being more easily accelerated at early cosmic epochs (Sect. 6.1). By investigating the dependence of the BAL kinematics with L_{Bol} , λ_{Edd} , we were able to exclude that the redshift evolution is due to different luminosity and/or accretion properties within the sample.

BAL outflows being more common and faster at $z \sim 6$ imply that strong BH feedback is likely occurring around this epoch, owing to the injection of large amounts of energy into the BH surroundings and in the galaxy medium, in agreement with expectations from galaxy evolution models ([van der Vlugt & Costa 2019](#); [Inayoshi et al. 2022](#)). However, the limited number of high-redshift quasars in our sample does not allow us to accurately probe the $z \gtrsim 4.5$ evolution of the BAL fraction on a timescale of 100-200 Myr. This hampers us from discriminating between a sudden or a smooth change of the BAL fraction with increasing redshift and, in turn, from assessing whether BH feedback is driving this evolution. Building a larger, absorption-unbiased sample of rest-frame optical bright quasars with high-quality optical and near-IR spectroscopy will be fundamental to observationally quantify the impact of BH feedback on early BH growth. By complementing this sample with high-frequency ALMA and JWST observations we will be able to measure the host-galaxy growth and to assess whether quasar feedback at $z \sim 6$ drives the onset of the symbiotic BH-and-galaxy evolution observed in the lower redshift Universe.

Acknowledgements: this work is based on observations collected at the European Organisation for Astronomical Research in the Southern Hemisphere under ESO large programme 1103.A-0817(A). Funding for SDSS and SDSS-II has been provided by the Alfred P. Sloan Foundation, the Participating Institutions, the National Science Foundation, the US Department of Energy, the National Aeronautics and Space Administration, the Japanese Monbukagakusho, the Max Planck Society and the Higher Education Funding Council for England. The SDSS website is <http://www.sdss.org/>. The SDSS is managed by the Astrophysical Research Consortium for the Participating Institutions. The Participating Institutions are the American Museum of Natural History, the Astrophysical Institute Potsdam, the University of Basel, the University of Cambridge, Case Western Reserve University, the University of Chicago, Drexel University, Fermilab, the Institute for Advanced Study, the Japan Participation Group, Johns Hopkins University, the Joint Institute for Nuclear Astrophysics, the Kavli Institute for Particle Astrophysics and Cosmology, the Korean Scientist Group, the Chinese Academy of Sciences (LAMOST), Los Alamos National Laboratory, the Max-Planck-Institute for Astronomy, the Max-Planck-Institute for Astrophysics, New Mexico State University, Ohio State University, the University of Pittsburgh, the University of Portsmouth, Princeton University, the United States Naval Observatory, and the University of Washington. M.B., C.F., and F.F. acknowledge support from the PRIN MIUR project ‘Black hole winds and the baryon life cycle of galaxies: the stone-guest at the galaxy evolution supper’, contract number 2017PH3WAT, and support from INAF under PRIN SKA/CTA 2016 FORECaST project. MG acknowledges partial support by HST GO-15890.020/023-A and the *BlackHoleWeather* program. K.Z. acknowledges support by Research Council Lithuania grant no. S-MIP-20-43. E.P.F. is supported by the international Gemini Observatory, a program of NSF’s NOIRLab, which is managed by the Association of Universities for Research in Astronomy (AURA) under a cooperative agreement with the National Science Foundation, on behalf of the Gemini partnership of Argentina, Brazil, Canada, Chile, the Republic of Korea, and the United States of America.

Facilities: VLT(UT2 X-shooter), Sloan

Software: python 3.8 ([Van Rossum & Drake 2009](#)), numpy ([Harris et al. 2020](#)), astropy ([Astropy Collaboration et al. 2013, 2018](#)), pandas ([McKinney et al. 2010](#); [Reback et al. 2020](#)), matplotlib ([Hunter 2007](#))

REFERENCES

Allen, J. T., Hewett, P. C., Maddox, N., Richards, G. T., & Belokurov, V. 2011, MNRAS, 410, 860, doi: [10.1111/j.1365-2966.2010.17489.x](https://doi.org/10.1111/j.1365-2966.2010.17489.x)

Arav, N., Liu, G., Xu, X., et al. 2018, ApJ, 857, 60, doi: [10.3847/1538-4357/aab494](https://doi.org/10.3847/1538-4357/aab494)

Astropy Collaboration, Robitaille, T. P., Tollerud, E. J., et al. 2013, A&A, 558, A33, doi: [10.1051/0004-6361/201322068](https://doi.org/10.1051/0004-6361/201322068)

Astropy Collaboration, Price-Whelan, A. M., Sipőcz, B. M., et al. 2018, AJ, 156, 123, doi: [10.3847/1538-3881/aabc4f](https://doi.org/10.3847/1538-3881/aabc4f)

Bañados, E., Venemans, B. P., Decarli, R., et al. 2016, ApJS, 227, 11, doi: [10.3847/0067-0049/227/1/11](https://doi.org/10.3847/0067-0049/227/1/11)

Banerji, M., Alaghband-Zadeh, S., Hewett, P. C., & McMahon, R. G. 2015, MNRAS, 447, 3368, doi: [10.1093/mnras/stu2649](https://doi.org/10.1093/mnras/stu2649)

Baskin, A., Laor, A., & Hamann, F. 2015, MNRAS, 449, 1593, doi: [10.1093/mnras/stv406](https://doi.org/10.1093/mnras/stv406)

Becker, G. D., Pettini, M., Rafelski, M., et al. 2019, ApJ, 883, 163, doi: [10.3847/1538-4357/ab3eb5](https://doi.org/10.3847/1538-4357/ab3eb5)

Becker, R. H., White, R. L., Gregg, M. D., et al. 2000, ApJ, 538, 72, doi: [10.1086/309099](https://doi.org/10.1086/309099)

Bianchi, S. 2008, A&A, 490, 461, doi: [10.1051/0004-6361:200810027](https://doi.org/10.1051/0004-6361:200810027)

Bischetti, M., Feruglio, C., D'Odorico, V., et al. 2022, Nature, 605, 244, doi: [10.1038/s41586-022-04608-1](https://doi.org/10.1038/s41586-022-04608-1)

Borguet, B. C. J., Arav, N., Edmonds, D., Chamberlain, C., & Benn, C. 2013, ApJ, 762, 49, doi: [10.1088/0004-637X/762/1/49](https://doi.org/10.1088/0004-637X/762/1/49)

Bosman, S. E. I., Davies, F. B., Becker, G. D., et al. 2021, arXiv e-prints, arXiv:2108.03699, <https://arxiv.org/abs/2108.03699>

Boutsia, K., Grazian, A., Fontanot, F., et al. 2021, ApJ, 912, 111, doi: [10.3847/1538-4357/abedb5](https://doi.org/10.3847/1538-4357/abedb5)

Bruni, G., Piconcelli, E., Misawa, T., et al. 2019, A&A, 630, A111, doi: [10.1051/0004-6361/201834940](https://doi.org/10.1051/0004-6361/201834940)

Byun, D., Arav, N., & Hall, P. B. 2022, ApJ, 927, 176, doi: [10.3847/1538-4357/ac503d](https://doi.org/10.3847/1538-4357/ac503d)

Cao Orjales, J. M., Stevens, J. A., Jarvis, M. J., et al. 2012, MNRAS, 427, 1209, doi: [10.1111/j.1365-2966.2012.22049.x](https://doi.org/10.1111/j.1365-2966.2012.22049.x)

Carniani, S., Gallerani, S., Vallini, L., et al. 2019, MNRAS, 489, 3939, doi: [10.1093/mnras/stz2410](https://doi.org/10.1093/mnras/stz2410)

Chehade, B., Carnall, A. C., Shanks, T., et al. 2018, MNRAS, 478, 1649, doi: [10.1093/mnras/sty690](https://doi.org/10.1093/mnras/sty690)

Chen, Z., He, Z., Ho, L. C., et al. 2022, Nature Astronomy, 6, 339, doi: [10.1038/s41550-021-01561-3](https://doi.org/10.1038/s41550-021-01561-3)

Coatman, L., Hewett, P. C., Banerji, M., et al. 2017, MNRAS, 465, 2120, doi: [10.1093/mnras/stw2797](https://doi.org/10.1093/mnras/stw2797)

Costa, T., Rosdahl, J., Sijacki, D., & Haehnelt, M. G. 2018, MNRAS, 473, 4197, doi: [10.1093/mnras/stx2598](https://doi.org/10.1093/mnras/stx2598)

Costa, T., Sijacki, D., Trenti, M., & Haehnelt, M. G. 2014, MNRAS, 439, 2146, doi: [10.1093/mnras/stu101](https://doi.org/10.1093/mnras/stu101)

Dai, X., Shankar, F., & Sivakoff, G. R. 2008, ApJ, 672, 108, doi: [10.1086/523688](https://doi.org/10.1086/523688)

Decarli, R., Walter, F., Venemans, B. P., et al. 2018, ApJ, 854, 97, doi: [10.3847/1538-4357/aaa5aa](https://doi.org/10.3847/1538-4357/aaa5aa)

Di Mascia, F., Gallerani, S., Behrens, C., et al. 2021, MNRAS, 503, 2349, doi: [10.1093/mnras/stab528](https://doi.org/10.1093/mnras/stab528)

Dunn, J. P., Arav, N., Aoki, K., et al. 2012, ApJ, 750, 143, doi: [10.1088/0004-637X/750/2/143](https://doi.org/10.1088/0004-637X/750/2/143)

Dunn, J. P., Crenshaw, D. M., Kraemer, S. B., & Trippe, M. L. 2010, ApJ, 713, 900, doi: [10.1088/0004-637X/713/2/900](https://doi.org/10.1088/0004-637X/713/2/900)

Duras, F., Bongiorno, A., Piconcelli, E., et al. 2017, A&A, 604, A67, doi: [10.1051/0004-6361/201731052](https://doi.org/10.1051/0004-6361/201731052)

Eilers, A.-C., Hennawi, J. F., Decarli, R., et al. 2020, ApJ, 900, 37, doi: [10.3847/1538-4357/aba52e](https://doi.org/10.3847/1538-4357/aba52e)

Elvis, M. 2000, ApJ, 545, 63, doi: [10.1086/317778](https://doi.org/10.1086/317778)

Farina, E. P., Schindler, J.-T., Walter, F., et al. 2022, arXiv e-prints, arXiv:2207.05113, <https://arxiv.org/abs/2207.05113>

Farrah, D., Urrutia, T., Lacy, M., et al. 2012, ApJ, 745, 178, doi: [10.1088/0004-637X/745/2/178](https://doi.org/10.1088/0004-637X/745/2/178)

Faucher-Giguère, C.-A., & Quataert, E. 2012, MNRAS, 425, 605, doi: [10.1111/j.1365-2966.2012.21512.x](https://doi.org/10.1111/j.1365-2966.2012.21512.x)

Fiore, F., Feruglio, C., Shankar, F., et al. 2017, A&A, 601, A143, doi: [10.1051/0004-6361/201629478](https://doi.org/10.1051/0004-6361/201629478)

Gallerani, S., Maiolino, R., Juarez, Y., et al. 2010, A&A, 523, A85, doi: [10.1051/0004-6361/201014721](https://doi.org/10.1051/0004-6361/201014721)

Ganguly, R., & Brotherton, M. S. 2008, ApJ, 672, 102, doi: [10.1086/524106](https://doi.org/10.1086/524106)

Ganguly, R., Brotherton, M. S., Cales, S., et al. 2007, ApJ, 665, 990, doi: [10.1086/519759](https://doi.org/10.1086/519759)

Gaspari, M. 2015, MNRAS, 451, L60, doi: [10.1093/mnrasl/slv067](https://doi.org/10.1093/mnrasl/slv067)

Gaspari, M., & Sadowski, A. 2017, ApJ, 837, 149, doi: [10.3847/1538-4357/aa61a3](https://doi.org/10.3847/1538-4357/aa61a3)

Gaspari, M., Tombesi, F., & Cappi, M. 2020, Nature Astronomy, 4, 10, doi: [10.1038/s41550-019-0970-1](https://doi.org/10.1038/s41550-019-0970-1)

Gaspari, M., Eckert, D., Ettori, S., et al. 2019, ApJ, 884, 169, doi: [10.3847/1538-4357/ab3c5d](https://doi.org/10.3847/1538-4357/ab3c5d)

Gibson, R. R., Jiang, L., Brandt, W. N., et al. 2009, ApJ, 692, 758, doi: [10.1088/0004-637X/692/1/758](https://doi.org/10.1088/0004-637X/692/1/758)

Giustini, M., Cappi, M., & Vignali, C. 2008, A&A, 491, 425, doi: [10.1051/0004-6361:200810363](https://doi.org/10.1051/0004-6361:200810363)

Glikman, E., Lacy, M., Urrutia, T., Djorgovski, G., & Mahabal, A. 2012, in American Astronomical Society Meeting Abstracts, Vol. 219, American Astronomical Society Meeting Abstracts #219, 209.03

Glikman, E., Lacy, M., LaMassa, S., et al. 2018, *ApJ*, 861, 37, doi: [10.3847/1538-4357/aac5d8](https://doi.org/10.3847/1538-4357/aac5d8)

Grazian, A., Giallongo, E., Boutsia, K., et al. 2022, *ApJ*, 924, 62, doi: [10.3847/1538-4357/ac33a4](https://doi.org/10.3847/1538-4357/ac33a4)

Guo, Z., & Martini, P. 2019, *ApJ*, 879, 72, doi: [10.3847/1538-4357/ab2590](https://doi.org/10.3847/1538-4357/ab2590)

Hall, P. B., Anderson, S. F., Strauss, M. A., et al. 2002, *ApJS*, 141, 267, doi: [10.1086/340546](https://doi.org/10.1086/340546)

Hamann, F., Chartas, G., Reeves, J., & Nardini, E. 2018, *MNRAS*, 476, 943, doi: [10.1093/mnras/sty043](https://doi.org/10.1093/mnras/sty043)

Harris, C. R., Millman, K. J., van der Walt, S. J., et al. 2020, *Nature*, 585, 357, doi: [10.1038/s41586-020-2649-2](https://doi.org/10.1038/s41586-020-2649-2)

Hemler, Z. S., Grier, C. J., Brandt, W. N., et al. 2019, *ApJ*, 872, 21, doi: [10.3847/1538-4357/aaf1bf](https://doi.org/10.3847/1538-4357/aaf1bf)

Hewett, P. C., & Foltz, C. B. 2003, *AJ*, 125, 1784, doi: [10.1086/368392](https://doi.org/10.1086/368392)

Hunter, J. D. 2007, *Computing in science & engineering*, 9, 90

Inayoshi, K., Haiman, Z., & Ostriker, J. P. 2016, *MNRAS*, 459, 3738, doi: [10.1093/mnras/stw836](https://doi.org/10.1093/mnras/stw836)

Inayoshi, K., Nakatani, R., Toyouchi, D., et al. 2022, *ApJ*, 927, 237, doi: [10.3847/1538-4357/ac4751](https://doi.org/10.3847/1538-4357/ac4751)

Ishibashi, W., Banerji, M., & Fabian, A. C. 2017, *MNRAS*, 469, 1496, doi: [10.1093/mnras/stx921](https://doi.org/10.1093/mnras/stx921)

Kato, N., Matsuoka, Y., Onoue, M., et al. 2020, *PASJ*, 72, 84, doi: [10.1093/pasj/psaa074](https://doi.org/10.1093/pasj/psaa074)

King, A. R., Pringle, J. E., & Hofmann, J. A. 2008, *MNRAS*, 385, 1621, doi: [10.1111/j.1365-2966.2008.12943.x](https://doi.org/10.1111/j.1365-2966.2008.12943.x)

Knigge, C., Scaringi, S., Goad, M. R., & Cottis, C. E. 2008, *MNRAS*, 386, 1426, doi: [10.1111/j.1365-2966.2008.13081.x](https://doi.org/10.1111/j.1365-2966.2008.13081.x)

Kurk, J. D., Walter, F., Fan, X., et al. 2007, *ApJ*, 669, 32, doi: [10.1086/521596](https://doi.org/10.1086/521596)

Laha, S., Reynolds, C. S., Reeves, J., et al. 2021, *Nature Astronomy*, 5, 13, doi: [10.1038/s41550-020-01255-2](https://doi.org/10.1038/s41550-020-01255-2)

Lai, S., Bian, F., Onken, C. A., et al. 2022, *MNRAS*, doi: [10.1093/mnras/stac1001](https://doi.org/10.1093/mnras/stac1001)

Lamastra, A., Menci, N., Maiolino, R., Fiore, F., & Merloni, A. 2010, *MNRAS*, 405, 29, doi: [10.1111/j.1365-2966.2010.16439.x](https://doi.org/10.1111/j.1365-2966.2010.16439.x)

Laor, A., & Brandt, W. N. 2002, *ApJ*, 569, 641, doi: [10.1086/339476](https://doi.org/10.1086/339476)

Maddox, N., Hewett, P. C., Warren, S. J., & Croom, S. M. 2008, *MNRAS*, 386, 1605, doi: [10.1111/j.1365-2966.2008.13138.x](https://doi.org/10.1111/j.1365-2966.2008.13138.x)

Maiolino, R., Oliva, E., Ghinassi, F., et al. 2004, *A&A*, 420, 889, doi: [10.1051/0004-6361:20035704](https://doi.org/10.1051/0004-6361:20035704)

Marconi, A., Risaliti, G., Gilli, R., et al. 2004, *MNRAS*, 351, 169, doi: [10.1111/j.1365-2966.2004.07765.x](https://doi.org/10.1111/j.1365-2966.2004.07765.x)

Mazzucchelli, C., Bañados, E., Venemans, B. P., et al. 2017, *ApJ*, 849, 91, doi: [10.3847/1538-4357/aa9185](https://doi.org/10.3847/1538-4357/aa9185)

McKinney, W., et al. 2010, in Proceedings of the 9th Python in Science Conference, Vol. 445, Austin, TX, 51–56

Menci, N., Fiore, F., Feruglio, C., et al. 2019, *ApJ*, 877, 74, doi: [10.3847/1538-4357/ab1a3a](https://doi.org/10.3847/1538-4357/ab1a3a)

Moe, M., Arav, N., Bautista, M. A., & Korista, K. T. 2009, *ApJ*, 706, 525, doi: [10.1088/0004-637X/706/1/525](https://doi.org/10.1088/0004-637X/706/1/525)

Murray, N., & Chiang, J. 1998, *ApJ*, 494, 125, doi: [10.1086/305183](https://doi.org/10.1086/305183)

Nanni, R., Vignali, C., Gilli, R., Moretti, A., & Brandt, W. N. 2017, *A&A*, 603, A128, doi: [10.1051/0004-6361/201730484](https://doi.org/10.1051/0004-6361/201730484)

Neeleman, M., Novak, M., Venemans, B. P., et al. 2021, *ApJ*, 911, 141, doi: [10.3847/1538-4357/abe70f](https://doi.org/10.3847/1538-4357/abe70f)

Negri, A., & Volonteri, M. 2017, *MNRAS*, 467, 3475, doi: [10.1093/mnras/stx362](https://doi.org/10.1093/mnras/stx362)

O’Leary, J. A., Moster, B. P., Naab, T., & Somerville, R. S. 2021, *MNRAS*, 501, 3215, doi: [10.1093/mnras/staa3746](https://doi.org/10.1093/mnras/staa3746)

Onken, C. A., Wolf, C., Bian, F., et al. 2022, *MNRAS*, 511, 572, doi: [10.1093/mnras/stac051](https://doi.org/10.1093/mnras/stac051)

Pâris, I., Petitjean, P., Aubourg, É., et al. 2018, *A&A*, 613, A51, doi: [10.1051/0004-6361/201732445](https://doi.org/10.1051/0004-6361/201732445)

Pensabene, A., Carniani, S., Perna, M., et al. 2020, *A&A*, 637, A84, doi: [10.1051/0004-6361/201936634](https://doi.org/10.1051/0004-6361/201936634)

Pezzulli, E., Valiante, R., & Schneider, R. 2016, *MNRAS*, 458, 3047, doi: [10.1093/mnras/stw505](https://doi.org/10.1093/mnras/stw505)

Pitchford, L. K., Hatziminaoglou, E., Feltre, A., et al. 2016, *MNRAS*, 462, 4067, doi: [10.1093/mnras/stw1840](https://doi.org/10.1093/mnras/stw1840)

Planck Collaboration, Ade, P. A. R., Aghanim, N., et al. 2016, *A&A*, 594, A13, doi: [10.1051/0004-6361/201525830](https://doi.org/10.1051/0004-6361/201525830)

Proga, D., & Kallman, T. R. 2004, *ApJ*, 616, 688, doi: [10.1086/425117](https://doi.org/10.1086/425117)

Proga, D., Stone, J. M., & Kallman, T. R. 2000, *ApJ*, 543, 686, doi: [10.1086/317154](https://doi.org/10.1086/317154)

Reback, J., McKinney, W., jbrockmendel, et al. 2020, pandas-dev/pandas: Pandas 1.1.3, v1.1.3, Zenodo, doi: [10.5281/zenodo.4067057](https://doi.org/10.5281/zenodo.4067057)

Reed, S. L., McMahon, R. G., Martini, P., et al. 2017, *MNRAS*, 468, 4702, doi: [10.1093/mnras/stx728](https://doi.org/10.1093/mnras/stx728)

Reichard, T. A., Richards, G. T., Hall, P. B., et al. 2003, *AJ*, 126, 2594, doi: [10.1086/379293](https://doi.org/10.1086/379293)

Richards, G. T., Fan, X., Newberg, H. J., et al. 2002, *AJ*, 123, 2945, doi: [10.1086/340187](https://doi.org/10.1086/340187)

Richards, G. T., Lacy, M., Storrie-Lombardi, L. J., et al. 2006, *ApJS*, 166, 470, doi: [10.1086/506525](https://doi.org/10.1086/506525)

Richards, G. T., Kruczak, N. E., Gallagher, S. C., et al. 2011, *AJ*, 141, 167, doi: [10.1088/0004-6256/141/5/167](https://doi.org/10.1088/0004-6256/141/5/167)

Rodríguez Hidalgo, P., Khatri, A. M., Hall, P. B., et al. 2020, *ApJ*, 896, 151, doi: [10.3847/1538-4357/ab9198](https://doi.org/10.3847/1538-4357/ab9198)

Runnoe, J. C., Brotherton, M. S., & Shang, Z. 2012, *MNRAS*, 426, 2677, doi: [10.1111/j.1365-2966.2012.21644.x](https://doi.org/10.1111/j.1365-2966.2012.21644.x)

Sadowski, A., & Gaspari, M. 2017, *MNRAS*, 468, 1398, doi: [10.1093/mnras/stx543](https://doi.org/10.1093/mnras/stx543)

Schindler, J.-T., Fan, X., McGreer, I. D., et al. 2019, *ApJ*, 871, 258, doi: [10.3847/1538-4357/aaf86c](https://doi.org/10.3847/1538-4357/aaf86c)

Schindler, J.-T., Farina, E. P., Bañados, E., et al. 2020, *ApJ*, 905, 51, doi: [10.3847/1538-4357/abc2d7](https://doi.org/10.3847/1538-4357/abc2d7)

Schneider, D. P., Hall, P. B., Richards, G. T., et al. 2007, *AJ*, 134, 102, doi: [10.1086/518474](https://doi.org/10.1086/518474)

Shen, Y., Richards, G. T., Strauss, M. A., et al. 2011, *ApJS*, 194, 45, doi: [10.1088/0067-0049/194/2/45](https://doi.org/10.1088/0067-0049/194/2/45)

Shen, Y., Wu, J., Jiang, L., et al. 2019, *ApJ*, 873, 35, doi: [10.3847/1538-4357/ab03d9](https://doi.org/10.3847/1538-4357/ab03d9)

Skrutskie, M. F., Cutri, R. M., Stiening, R., et al. 2006, *AJ*, 131, 1163, doi: [10.1086/498708](https://doi.org/10.1086/498708)

Smette, A., Sana, H., Noll, S., et al. 2015, *A&A*, 576, A77, doi: [10.1051/0004-6361/201423932](https://doi.org/10.1051/0004-6361/201423932)

Torrey, P., Hopkins, P. F., Faucher-Giguère, C.-A., et al. 2020, *MNRAS*, 497, 5292, doi: [10.1093/mnras/staa2222](https://doi.org/10.1093/mnras/staa2222)

Trakhtenbrot, B. 2021, in Nuclear Activity in Galaxies Across Cosmic Time, ed. M. Pović, P. Marziani, J. Masegosa, H. Netzer, S. H. Negu, & S. B. Tessema, Vol. 356, 261–275, doi: [10.1017/S1743921320003087](https://doi.org/10.1017/S1743921320003087)

Tripodi, R., Feruglio, C., Fiore, F., et al. 2022, arXiv e-prints, arXiv:2207.03314. <https://arxiv.org/abs/2207.03314>

Trump, J. R., Hall, P. B., Reichard, T. A., et al. 2006, *ApJS*, 165, 1, doi: [10.1086/503834](https://doi.org/10.1086/503834)

Urrutia, T., Lacy, M., & Becker, R. H. 2008, *ApJ*, 674, 80, doi: [10.1086/523959](https://doi.org/10.1086/523959)

van der Vlugt, D., & Costa, T. 2019, *MNRAS*, 490, 4918, doi: [10.1093/mnras/stz2944](https://doi.org/10.1093/mnras/stz2944)

Van Rossum, G., & Drake, F. L. 2009, Python 3 Reference Manual (Scotts Valley, CA: CreateSpace)

Venemans, B. P., Decarli, R., Walter, F., et al. 2018, *ApJ*, 866, 159, doi: [10.3847/1538-4357/aadf35](https://doi.org/10.3847/1538-4357/aadf35)

Vietri, G., Piconcelli, E., Bischetti, M., et al. 2018, *A&A*, 617, A81, doi: [10.1051/0004-6361/201732335](https://doi.org/10.1051/0004-6361/201732335)

Vietri, G., Misawa, T., Piconcelli, E., et al. 2022, arXiv e-prints, arXiv:2205.06832. <https://arxiv.org/abs/2205.06832>

Vito, F., Brandt, W. N., Bauer, F. E., et al. 2019, *A&A*, 630, A118, doi: [10.1051/0004-6361/201936217](https://doi.org/10.1051/0004-6361/201936217)

Volonteri, M., & Rees, M. J. 2006, *ApJ*, 650, 669, doi: [10.1086/507444](https://doi.org/10.1086/507444)

Wang, F., Yang, J., Fan, X., et al. 2018, *ApJL*, 869, L9, doi: [10.3847/2041-8213/aafl1d2](https://doi.org/10.3847/2041-8213/aafl1d2)

—. 2019, *ApJ*, 884, 30, doi: [10.3847/1538-4357/ab2be5](https://doi.org/10.3847/1538-4357/ab2be5)

—. 2021a, *ApJL*, 907, L1, doi: [10.3847/2041-8213/abd8c6](https://doi.org/10.3847/2041-8213/abd8c6)

Wang, F., Fan, X., Yang, J., et al. 2021b, *ApJ*, 908, 53, doi: [10.3847/1538-4357/abcc5e](https://doi.org/10.3847/1538-4357/abcc5e)

Warren, S. J., Hambly, N. C., Dye, S., et al. 2007, *MNRAS*, 375, 213, doi: [10.1111/j.1365-2966.2006.11284.x](https://doi.org/10.1111/j.1365-2966.2006.11284.x)

Wethers, C. F., Kotilainen, J., Schramm, M., & Schulze, A. 2020, *MNRAS*, 498, 1469, doi: [10.1093/mnras/staa2017](https://doi.org/10.1093/mnras/staa2017)

Weymann, R. J., Morris, S. L., Foltz, C. B., & Hewett, P. C. 1991, *ApJ*, 373, 23, doi: [10.1086/170020](https://doi.org/10.1086/170020)

Wolf, C., Hon, W. J., Bian, F., et al. 2020, *MNRAS*, 491, 1970, doi: [10.1093/mnras/stz2955](https://doi.org/10.1093/mnras/stz2955)

Wright, E. L., Eisenhardt, P. R. M., Mainzer, A. K., et al. 2010, *AJ*, 140, 1868, doi: [10.1088/0004-6256/140/6/1868](https://doi.org/10.1088/0004-6256/140/6/1868)

Xu, X., Zakamska, N. L., Arav, N., Miller, T., & Benn, C. 2020, *MNRAS*, 495, 305, doi: [10.1093/mnras/staa1142](https://doi.org/10.1093/mnras/staa1142)

Yang, J., Wang, F., Fan, X., et al. 2021, *ApJ*, 923, 262, doi: [10.3847/1538-4357/ac2b32](https://doi.org/10.3847/1538-4357/ac2b32)

Zeilig-Hess, M., Levinson, A., Xu, X., & Arav, N. 2020, *MNRAS*, 491, 4325, doi: [10.1093/mnras/stz3352](https://doi.org/10.1093/mnras/stz3352)

Zhang, S., Wang, H., Wang, T., et al. 2014, *ApJ*, 786, 42, doi: [10.1088/0004-637X/786/1/42](https://doi.org/10.1088/0004-637X/786/1/42)

Zhu, Y., Becker, G. D., Bosman, S. E. I., et al. 2022, *ApJ*, 932, 76, doi: [10.3847/1538-4357/ac6e60](https://doi.org/10.3847/1538-4357/ac6e60)

Zhu, Y. L., Lund, K. A., Barnes, J., et al. 2021, *ApJ*, 906, 94, doi: [10.3847/1538-4357/abc69e](https://doi.org/10.3847/1538-4357/abc69e)

Zubovas, K., & King, A. 2012, *ApJL*, 745, L34, doi: [10.1088/2041-8205/745/2/L34](https://doi.org/10.1088/2041-8205/745/2/L34)

—. 2013, *ApJ*, 769, 51, doi: [10.1088/0004-637X/769/1/51](https://doi.org/10.1088/0004-637X/769/1/51)

—. 2021, *MNRAS*, 501, 4289, doi: [10.1093/mnras/stab004](https://doi.org/10.1093/mnras/stab004)

APPENDIX

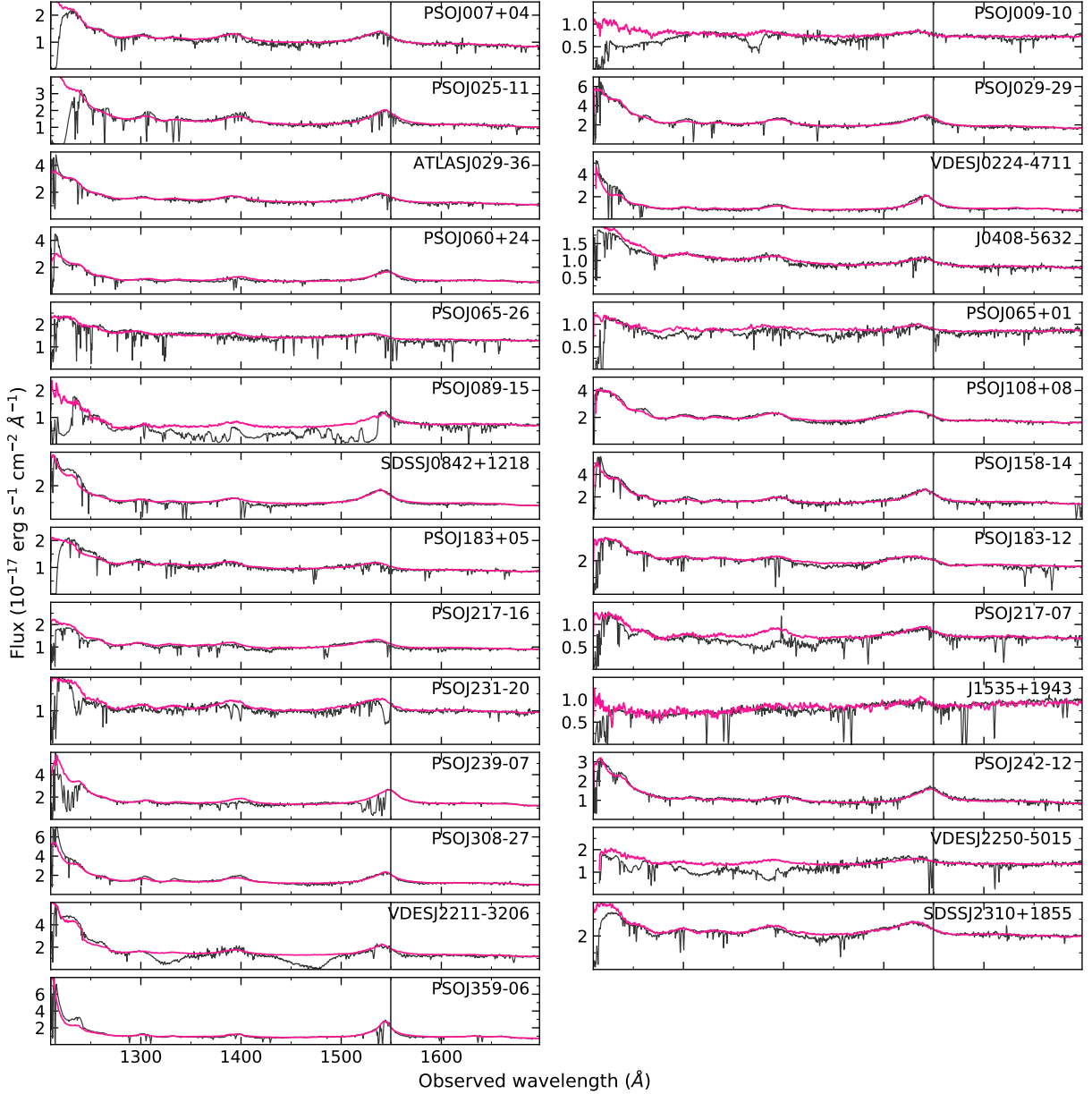


Figure 11. X-Shooter spectra of the $5.8 < z < 6.6$ quasars in our sample (black curves), binned to 150 km s^{-1} . Composite templates, used to estimate the intrinsic quasar emission are shown by the magenta curve. The vertical line indicates the rest-frame wavelength of C IV.

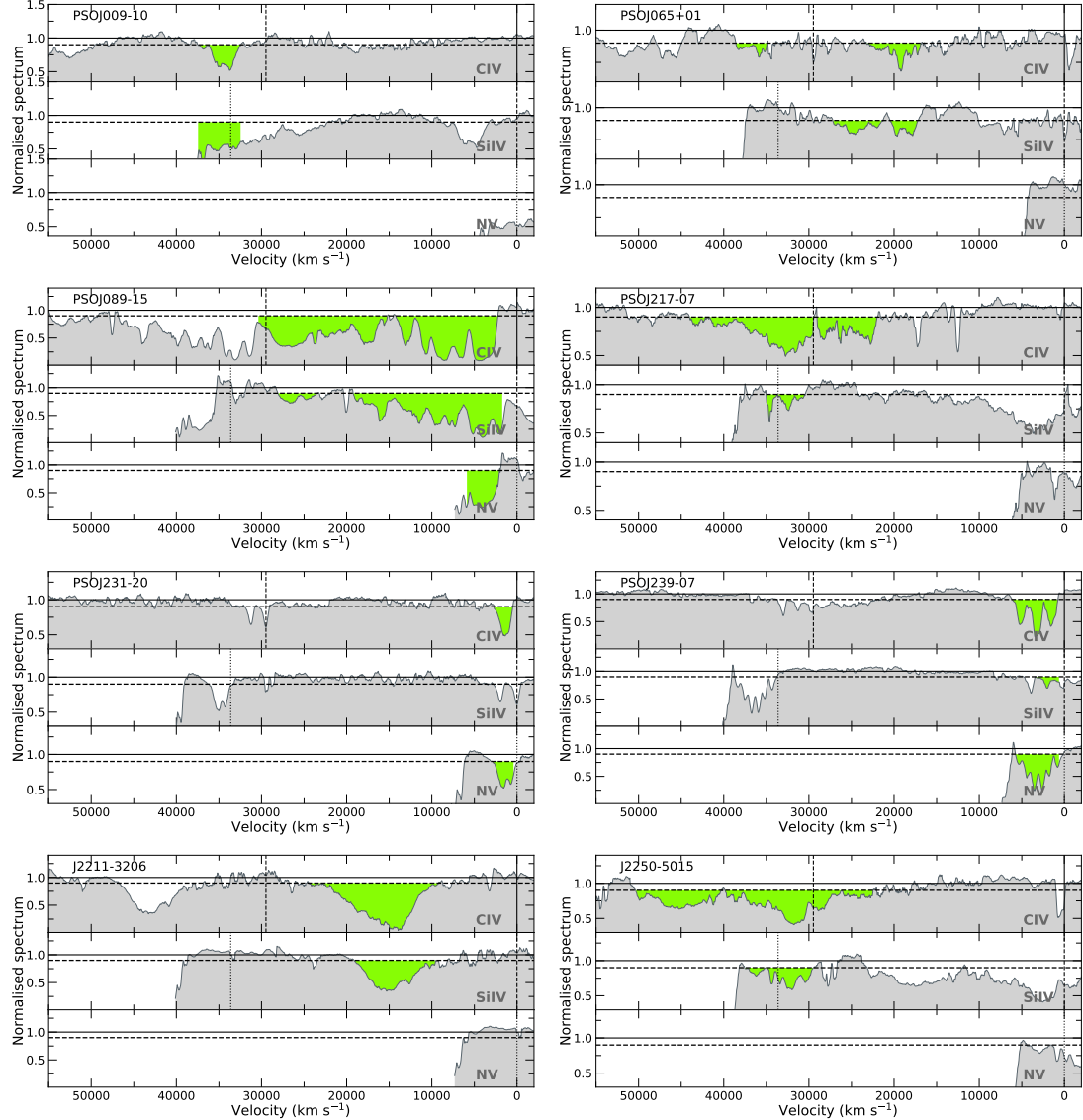


Figure 12. Normalised spectra for the BAL quasars identified in the $5.8 < z < 6.6$ sample, smoothed to 500 km s^{-1} . The velocity axis in each panel is relative to the rest-frame wavelength of the ionic species indicated by the label. Vertical solid, dashed, and dotted lines indicate the velocity associated with C IV, Si IV, and N V emission lines, respectively. The solid(dashed) horizontal line represents a flux level of 1.0(0.9). BAL troughs, corresponding to a flux level < 0.9 (Eq. 1), are highlighted as green shaded areas.